Hydrothermal equilibria and ore formation

Bortnikov N.S.[1], Kryazhev S.G.[2], Gorelikova N.V.[1], Smirnov S.Z.[3], Gonevchuk V.G.[4], Semenyak B.I.[4]., Dubinina E.O.[1]., Sokolova E.N.[3] The physicochemical conditions of tin deposit formation from the Badzhal ore district (Priamurye, Russia). UDC 553.21/.24

[1]Institute of Geology of Ore Deposits, Petrography, Mineralogy and Geochemistry, RAS, Moscow (bns@igem.ru, ngor@igem.ru);
[2] Central Geological Research Institute for Nonferrous and Precious Metals, Moscow, (S34@mail.ru);
[3 3]Institute of Geology and Mineralogy Novosibirsk, (ssmr@igm.nsc.ru);
[4]Far East Geological Institute RAS, Vladivostok, (Gonevchuk@fegi.ru)

Abstract. Based on the study of melt, combined fluid–melt and fluid inclusions and oxygen isotopes in quartz of the Urmi massive granite from the Badzhal volcanoplutonic zone and minerals from ore zones, physicochemical conditions of the formation of the Pravo-Urmi and Blizhnee tin–tungsten deposits have been revealed.

Keywords: *Badzhal, tin–tungsten deposits, melt, fluid, fluid–melt inclusions, thermobaric geochemistry, oxygen isotopes, ore formation conditions.*

The Badzhal volcanic zone is located in the central Khingan–Okhotsk magmatic belt at the western margin of the Jurassic accretionary prism in the Badzhal terrain within the Tan-Lu fault system. Several granitoid plutons exposed in this zone are considered projections of the single Badzhal cryptobatholith. The Verkhne-Urmi granitoid pluton accommodating the Pravo-Urmi deposit is the largest projection (350 km^2). (Fig. 1). The pluton comprises medium- to coarse-grained biotite granites that grade into porphyric granites and granite porphyres near contact zones. In terms of chemistry, granites of the pluton match the calc-alkaline alaskitic granites. Based on the ratio of trivalent and bivalent forms of Fe (0.35–0.45) and the prevalence of ilmenite over magnetite among accessories, the granites are assigned to the reduced (ilmenite) type. Based on the isotope-geochronological data, age of rocks of this pluton is estimated at 96 ± 1 Mya.

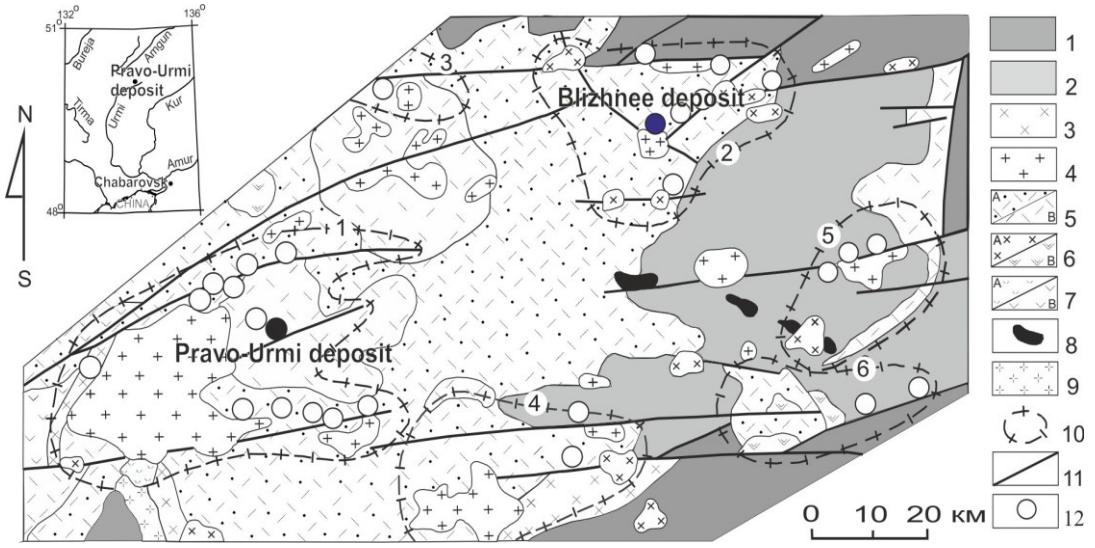

Fig.1. Geological structure (adapted from Komsomol'skaya regional geological office)
1 – Cretaceous deposits; 2 – Paleozoic terrigfenic-siliceous deposits; 3 – metamorphic deposits of Burea massif; 4 – biotite leucrocratic granites; 5 - rhyiolitests, rhyodacites of Badzhal volcanic complex: А - mantle, Б - extrusive; 6 – trakhyandesites (А) and gabbro-monzonite-diorites, granites of Silinka magmatic complex (Б); 7 - andesites of Lakskiy magmatic complex; 8 – alkali basalts, picrites of Dayn complex; 9 – Paleozoic granitoids; 10 – ore clusters: 1 – Verkhne-Urmi, 2 – Verkne-Badzhal, 3 - talidzhakskyi, 4 - Yarapskiy, 5 - Sutuingskiy, 6 – Yakun'skiy; 11 - faults: 1 - Badzhal, 2 – Axis of Badzhal, 3 – Pravo-Urmi, 4 - Verknesynchuginskiy, 5 - Kolbakan, 6 - Sutuingskiy, 7 - Kholodnyi, 8 - Azuritovyi, 9 - Granitovyi; 12 – deposits and ore occurences

This zone incorporates numerous occurrences of different metals (Sn, W, Mo, Cu, Pb, Zn, Hg and others) grouped into six (Verkhne-Urmi, Gerba, Verkhne-Badzhal, Syutyuinga, Yakun and Yarap ore nodes with different types of mineralization (Ognyanov, 1986). Ore mineralization within the nodes are genetically and paragenetically associated with volcanic domes (Verkhne-Urmi biotite granite pluton; Gerba extrusive dome; Badzhal–Bukam fissure intrusion group; and Syutyuinga, Yakun and Yarap granite plutons) including felsic intrusive and extrusive rocks in the core (Rodionov, 2005).

The largest and best-studied Verkhne-Urmi and Verkhne-Badzhal ore nodes are confined to the ancient extended Badzhal fault in the axial sector of the volcanic zone. The Verkhne-Urmi ore node is

located in the southwestern part of the ore district. This ore node is confined spatially to a volcanic dome, the core of which accommodates the Verkhne-Urmi biotite granite pluton controlled by the ancient northeastern Badzhal fault at its junction with no less ancient sublatitudinal faults (Os Badzhala, Pravo-Urmi and Verkhne-Synchuga). The western contact zone of pluton exposes a package of Devonian metamorphosed limestones, calcareous sandstones and siltstones replaced by pyroxene–garnet skarns with the superimposed tin–sulfide mineralization. The granite pluton is crosscut by numerous quartz veins, quartz–muscovite and quartz–topaz greisens (with cassiterite, wolframite, arsenopyrite, chalcopyrite and bismuth minerals), as well as pegmatoid molybdenite-bearing quartz–feldspar veins in some places (exo- and endocontact zones of pluton).

The eastern low-angle contact of the Verkhne-Urmi granite pluton accommodates the Pravo-Urmi tungsten–tin deposit confined to a thick and extended siderophyllite metasomatic zone on the hanging wall of the Pravo-Urmi granite porphyre dike. The sublatitudinal metasomatic zone is confined to the central Urmi caldera filled with a large extrusion (laccolith) of crystalline ignimbrites in the sublatitudinal fold zone on the hanging wall of the granite porphyre dike (Semenyak et al., 2006). The unique (in terms of reserves) orebody of the Pravo-Urmi deposit represents a linear stockwork (thickness 4-17 m, length 2400 and 900 m along the strike and dip, respectively). The stockwork is composed of numerous siderophyllite–quartz–topaz veins and veinlets with patches of cassiterite and arsenopyrite, as well as rare large lenses of the Sn-bearing quartz–topaz greisens. The veins are often crosscut by tourmaline veinlets with chalcopyrite and arsenopyrite. In the eastern watershed areas of the deposit, the ore stockwork is composed mainly of

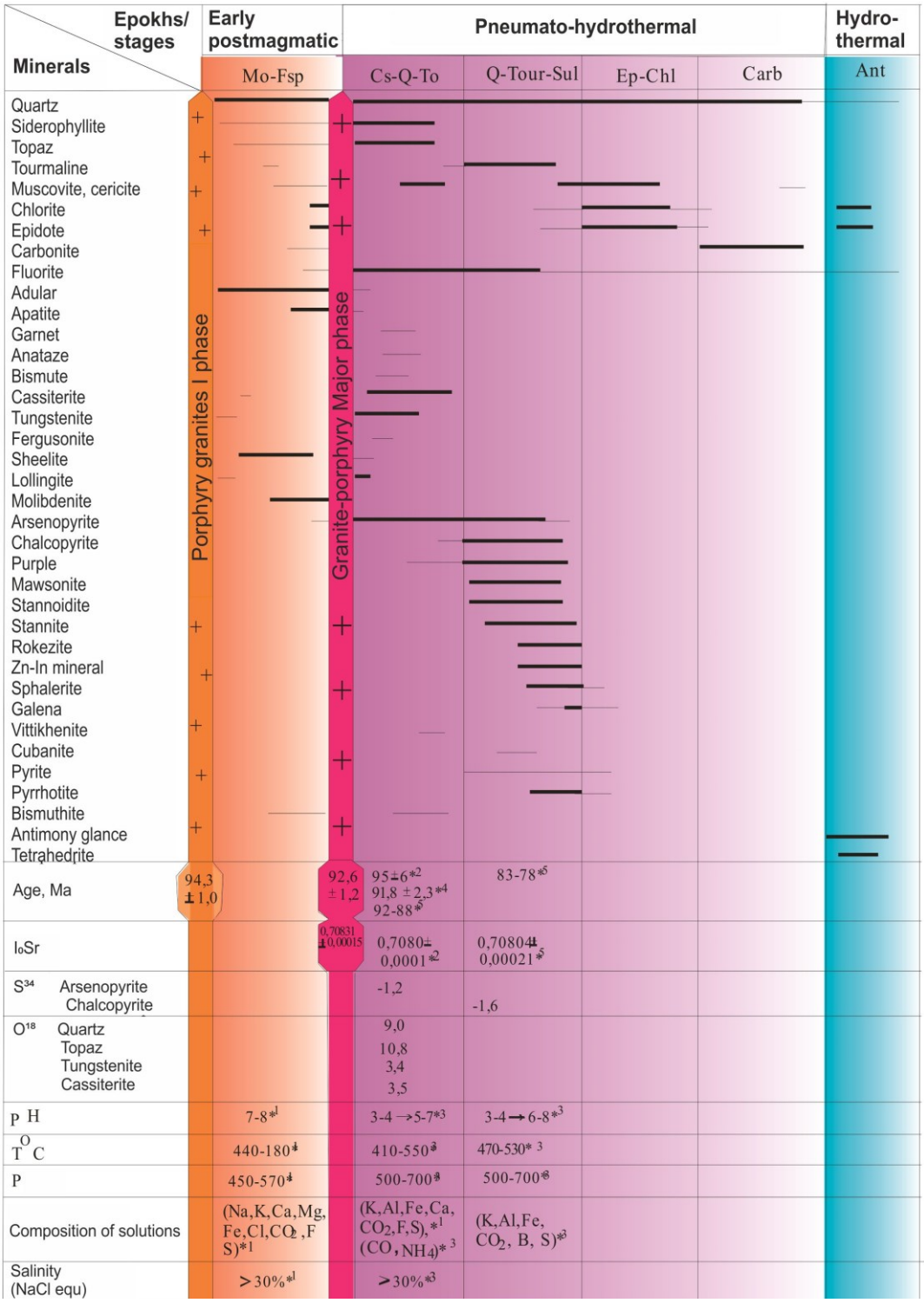

Fig. 2. The pattern of generation stage and mineral parageneses from Pravo-Urmi deposit
Mo – molibdenite; Fsp – feldspar; Cs – cassiterite; Q – quartz; To – topaz; Tour – tourmaline; Sul – sulphides; Ep – epidote; Chl – chlorite; Carb – carbonates; Ant – antimonite.

thick metasomatic quartz tourmalinite veins with abundant copper mineralization, Cu–Fe sulfostannates and subordinate cassiterite. In the distal eastern area of the granite pluton, the ore zone can only be traced on the surface based on thin quartz–chlorite veinlets (with rare xenogenic cassiterite) accompanied by epidote–chlorite alterations of the host siderophyllite metasomatites (Semenyak, 2006).

The Pravo-Urmi deposit was formed in three phases (Fig. 2). Among them, the earliest postmagmatic (molybdenite–feldspar) and late hydrothermal (antimonite) phases are related to a single mineralization stage, whereas the main productive (pneumatolitic-hydrothermal) phase includes four stages. The major commercial W–Sn mineralization is assigned to the earliest stage of the productive phase. Products of the earliest stage are represented by the pneumatolitic-hydrothermal veins and metasomatic bodies of granular topaz and fluorite, with interstices filled by quartz and siderophyllite. Isolated garnet and anatase grains occur in some places. Vein selvages are often emphasized by the fine flaky siderophyllite. The vein mass includes a chaotic distribution of cassiterite patches and dissemination, wolframite lamellas, and large arsenopyrite patches and stringers. Rare components are represented by scheelite, fergusonite, native bismuthinite and native bismuth. The present paper is dedicated to the study of physicochemical constraints of this mineralization stage.

The northeastern area of the ore district accommodates the Verkhne-Badzhal ore node with the Blizhnee deposit at the center. The Blizhnee ore field (Fig. 1) comprises the Upper Cretaceous intermediate and felsic volcanic rocks that make up a flat-lying package in the Permian–Carboniferous volcanosedimentary rock sequence. The sedimentary and volcanic rocks are intruded by subvolcanic bodies of andesidacites, dacites, phenocrystal rhyolites, quartz andesites and granite porphyres. One such body composed of andesidacites, dacites and phenocrystal rhyolites accommodates orebodies of the Yubileinaya zone, the main ore zone in the Blizhnee deposit. A large subintrusive granite porphyre dike intersects the deposit from the southwest to northeast. Exo- and endocontact zones of the dike include the slightly stanniferous Liparitovaya zone. The proximal southeastern area of the deposit is marked by the exposure of a small pluton of medium-grained porphyric granites that grade into the fine-grained leucocratic varieties near the endocontact.

The major ore-hosting structures of the deposit are represented by low-angle shear fissures (Yubileinaya, Lunokhod, Akkordnaya and Azuritovaya ore zones). The fissures are filled with numerous veinlets making up ore zones up to 300 m long and 4.5 m thick. The deposit is marked by a great mineral diversity of ore zones.

For example, the Akkordnaya zone is composed of siderophyllite–quartz–chlorite veins; the Azuritovaya and Lunokhod zones have the quartz–tourmaline composition; the Yubileinaya zone is composed of feldspar–quartz veins; and the Liparitovaya zone has the greisen (quartz–muscovite) composition. The Sn content is low in the majority of these zones.

The Yubileinaya zone is marked by the largest size and highest Sn content. The zone includes several low-angle contiguous veins and numerous veinlets. The veins are composed mainly of quartz that cements clasts of the silicified, K-feldspathized and sericitized rhyodacites. Cassiterite is mainly concentrated on the hanging wall of veins and sometimes disseminated over the whole vein mass. Cassiterite–quartz or cassiterite-only veinlets diverge from the main vein to host rocks. The ore veins and veinlets include fluorite, carbonate, galena and pyrite. The subordinate components in ores are represented by albite, orthoclase and intensely corroded quartz along with sericite, muscovite and tourmaline clusters. Near the contact with ore veins and veinlets, the host rhyodacites and their clasts in the vein material are altered into the lepido- to granoblastic sericite and orthoclase aggregates.

The main aim of our paper is to present the results of natural experiment based on scrutinization of the Badzhal Sn-bearing ore-magmatic system and to unravel physicochemical constraints of the deposition of Sn, W, and associated metals based on the study of melt and gas–liquid inclusions, as well as oxygen isotopes, in quartz and other minerals from the granitoid rocks and ore zones.

Urmi granites. The igneous quartz of these granites contain the primary melt, fluid and combined fluid–melt inclusions that often occur together as small isolated clusters (Fig.3), testifying to a heterogeneous mineral-forming medium composed of the silicate melt and magmatogenic fluid during the entrapment of inclusions.

Melt inclusions in the granite-hosted quartz are filled completely with an aggregate of crystalline phases. The homogenization temperature of melt inclusions does not exceed 650–680°C. The study of glass inclusions observed after the chilling revealed that ore-bearing fluids of the Badzhal system were formed during the crystallization of felsic melts with a moderate content of alumina, normal content of alkalis and elevated contents of H_2O (up to 8%), Cl (~0.1%) and F (~0.4%).

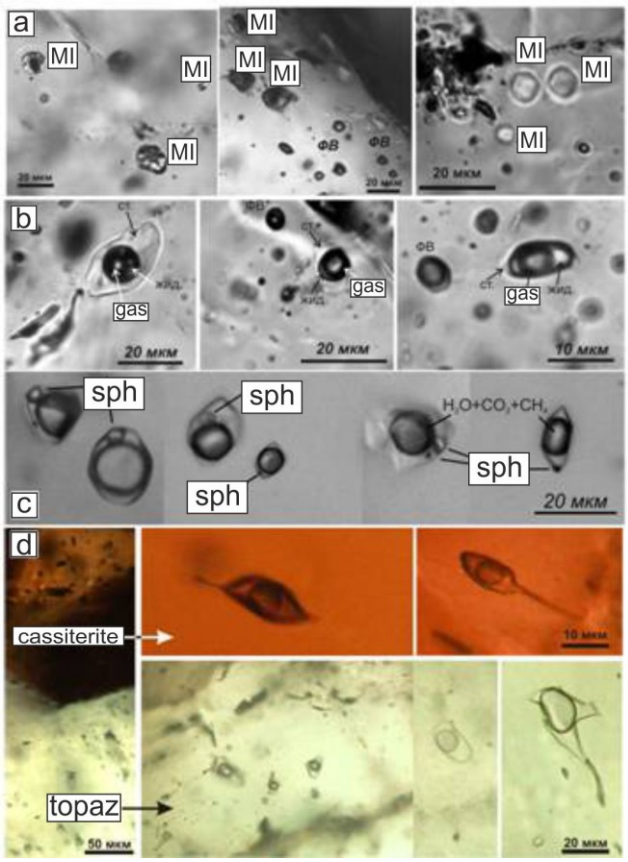

Fig. 3. (a–c) Inclusions in the granite-hosted quartz from the Verkhne-Urmi pluton: (a) melt (MI) and fluid (FI) inclusions (the right side shows homogeneous glass inclusions after heating in autoclave at 650°C); (b) fluid–melt inclusions with a variable proportion of silicate glass, water–salt fluid and vapor (gas) after heating in autoclave at 650°C; (c) fluid inclusions with solid subsidiary phases (sph.); (d) fluid inclusions in minerals from ore veins of the Pravo-Urmi deposit.

Primary fluid inclusions in the granite-hosted quartz are fractionated into two-phase types: gas–liquid (type 1); significantly gaseous with insoluble subsidiary phases (type 2). Based on the microthermometric data (Table 1), the fluid phase was extracted from the melt mainly as supercritical water–salt solution with the following parameters: density ~0.6 g/cm^3, salinity 9–19 wt % NaCl-equiv, and variable amount of the carbon-bearing gases (CO_2 and CH_4) (Rodder, 1987). The bulk analysis of inclusions is determined with the method of water extract (Kryazhev et al., 2006), in quartz from sample BG-82 revealed the following proportions of the major components: (0.72Na, 0.16K, 0.09Ca, 0.03Mg)/(0.93Cl, 0.07F). Trace elements are as follows (mg/kg H_2O): As (1186), B (174), Li (462), Rb (34), Cs (22), Sr (21), Zn (51), Cu (11), Mn (143). Based on the homogenization temperature discrepancy of fluid and melt inclusions, pressure during the entrapment of inclusions was 1.2 kbar.

Table 1. Parameters of fluid inclusions from magmatic and hydrothermal minerals

№ samples	Type of FI (mineral)	*N*	Temperature of phase change, °C				C of salts, wt.*% NaCl-equ.*
			$T_э$	$T_п$/*Л (Hh)*	$T_п$ *NaCl*	T_{gom} *(phase)*	
Primary inclusions in magmatic quartz							
BG-82	1 (Q)	15	undefined	–5.9±0.1	-	440–455 (к)	9.0
BG-25	2 (Q)	25	–31.5	–11…–15	-	450–470 (г)	15.0–18.6
Pravo-Urmi deposit. Quartz-cassiterite-topaz veins in greizens							
U-143-88	1 (TG)	15	–28	–6.0±0.2	-	430–450 (liq)	9.3
U-2-87	1 (T)	25	–29.5	–8.1±0.1	-	370–380 (liq)	11.8
	1 (Q)	43	–27.5	–7.8±0.1	-	370–380 (liq)	11.5
	1 (K)	7	–27…–30	–8.5±0.1	-	370–380 (liq)	12.1
Blizhnee deposit. Quartz-cassiterite vein							
BSHU-1-14	1 (Q)	5	undefined	–9.2±0.2	-	400–420 (liq)	13.1±0.2
	3 (Q)	3	–45	–33 (Hh)	280–290	395–405 (liq)	36.7–37.4
	3 (Q)	15	–45	–30 (Hh)	230–255	330–350 (liq)	33.5–35.0

Minerals: Q – quartz, TG – topaz in greizens, T – topaz in veins. K – cassiterite. Type FI: 1 – two-phase vapour-fluid ones, 2 – essentially gaseous ones with insoluble daughter phases, 3 – multi-phase inclusions with sodium chloride crystal. Temperature: Te – eutectic, TпЛ – ice melting, (Hh) – melting of hydrohalite, Tgom – homogenization of liquid phase (liq – in liquid, к – in a critical condition, g– in gas), Тп NaCl – solution of sodium chloride crystal (line – sodium chloride is absence). n/d – phase change is showed unclearly. N – number of examined inclusions.

Pravo-Urmi deposit. Topaz crystals from greisens (Table 1), sample U143-88 contain primary inclusions that are highly similar, based on the microthermometric characteristics, to the granite-hosted counterparts. They contain the alkali-chloride solution with a concentration of ~9% NaCl-equiv and homogenize at 430–450°C into the liquid phase (near the critical point). Gresisenization was accomplished obviously with the involvement of magmatogenic fluid at the early postmagmatic stage. Similarity of the homogenization temperature of minerals under consideration suggests a similarity of PT conditions during the entrapment of primary inclusions in the quartz and topaz of granites and greisens, respectively. The upper limit for the greisens is constrained by a temperature of 550°C and pressure of ~1 kbar. Based on the bulk analysis of solutions, the main components of inclusions have the following mole proportions: (0.86Na, 0.1K, 0.03Ca, 0.01Mg)/(0.5Cl, 0.2F, 0.3HCO_3). Trace elements are

Table 2. Composition of fluid inclusions (according to data of bulk analysis)

№ sample	BG-82	U-143-88	BSHU1-14
Object	Granite (Badzhal).	Pravo-Urmi	Blizhnee
Mineral	Quartz	Topaz	Quartz
H_2O in mineral, ppm	642.9	906.6	590.1
Carbon gases, mole / kg H_2O			
CO_2	0.51	0.21	0.16
CH_4*	0.25	0.29	0.10
Main components, g / kg H_2O			
Cl	43.85	7.79	39.38
F	1.74	1.68	<1
HCO_3	0.00	7.79	67.00
Na	13.64	8.38	45.31
K	4.98	1.56	3.55
Ca	2.92	0.47	3.16
Mg	0.65	0.13	0.05
Σ salts	67.8	28.2	160.0
Cl/F	25.2	4.6	>40
Trace elements, мg /kg H_2O			
Br	390.1	168.1	209.7
B	174.2	1625.5	957.4
Li	462.1	220.7	16.8
Rb	33.5	42.5	42.1
Cs	21.6	64.9	171.7
Sr	21.4	17.2	13.0
Ba	2.9	5.2	1.6
As	1185.7	56.8	53.8
Sb	11.7	14.8	54.3
Ge	0.1	0.6	4.8
Cu	11.1	0.0	1.1
Zn	50.7	0.0	0.0
Mo	0.2	3.8	7.7
W	0.8	22.6	15.4
Sn	0.0	0.0	13.0
Tl	0.2	173.2	1.2
Ni	1.4	2.2	6.4
Mn	142.7	317.2	606.6
Mole fractions			
Na	0.72	0.86	0.92
K	0.16	0.10	0.04
Ca	0.09	0.03	0.04
Mg	0.03	0.01	0.00
Cl	0.93	0.50	0.50
HCO_3	0.00	0.30	0.50
F	0.07	0.20	<0.02
Mole ratios			
Na / K	4.6	9.1	21.7
Na+K / Ca+Mg	7.2	23.5	25.4
HCO_3 / Cl+F	0.0	0.4	0.9
CO_2 / CH_4*	2.0	0.7	1.6

CH_4* - sum of hydrocarbons calculated as CH_4, Fe ,V, Cr, Co, U, Hg, Au, Ag, Bi, Pb, Cd, SO_4 are not detected.

as follows (mg/kg H_2O): B (1625), Li (220), Mn (317), Br (168), Rb (43), Cs (65), Sr (17), W (23), Mo (4), As (57), Tl (173). Thus, despite retention of the general geochemical specialization of magmatogenic solutions, their evolution was accompanied by changes in proportions of both major salt components and trace elements.

In *ore veins*, we examined fluid inclusions entrapped in the major minerals (topaz, quartz and cassiterite) of the productive assemblage (Fig. 3d). All inclusions are primary. They make up isolated clusters unrelated to fissures. Relatively large vacuoles are encountered in some places. Inclusions associated with arsenopyrite contain a tiny subsidiary ore phase. Microthermometric studies revealed that all minerals of this assemblage were formed at a similar temperature range from a common alkali-chloride solution (homogenization temperature of inclusions 370–380°C, eutectics temperature –27…–30°C). The ice melting temperature shows a small variation (–7.8…–8.5°C) and corresponds to a salinity of 11.8 ± 0.3% NaCl-equiv. Pressure in the inclusions at the homogenization temperature is ~200 bar. Assuming the continuity and temporal conjugation of processes of the formation of greisens and ore veins, homogenization temperature of inclusions should be corrected for a pressure of ~1 kbar. Under such conditions, the upper temperature limit for the crystallization of minerals will be 480°C.

Blizhnee deposit. Inclusions were detected here in quartz closely associated cassiterite. Quartz makes up well-developed prismatic crystals with numerous growth zones. Cassiterite is virtually nontransparent and concentrated as overgrowth on quartz crystals at the contact with host rocks. Based on the timing, they are divided into: (i) primary inclusions distributed regularly relative to growth zones of quartz crystals and (ii) pseudosecondary inclusions healing short cracks.

Based on the composition at room temperature, the inclusions are divided into: two-phase (gas–liquid) inclusions (type 1); significantly gaseous (water vapor) inclusions (type 2); and multiphase

inclusions with solid subsidiary phases (type 3).

Inner zones of crystals only contain the two-phase fluid inclusions (Table 1, type 1). At room temperature, they contain the water–salt solution and vapor bubble. Salinity of the water solution is 13 wt % NaCl-equiv, and the inclusions homogenize into the liquid phase at 400–420°C.

Outer zones of crystals contain both primary and pseudosecondary inclusions of two types: significantly gaseous inclusions (type 2) containing vapor and a small amount of liquid; multiphase inclusions (type 3) containing gas bubble, water–salt solution, crystal halite and one or two insoluble subsidiary phases. Based on the incipient ice melting temperature (–45°C) for type 3 inclusions, the entrapped fluid contains NaCl, KCl and $CaCl_2$. Based on the bulk analysis of solutions, mole proportions of the major components in the inclusions are as follows: (0.92Na, 0.04K, 0.04Ca)/(0.5Cl, $0.5HCO_3$). Trace elements are as follows (mg/kg H_2O): B (957), Li (17), Mn (607), Br (210), Rb (42), Cs (172), Sr (13), W (15), Mo (8), Sn (13), As (54), Ge (5).

Confinement of the brine (type 3) and vapor (type 2) inclusions to the same growth zones of quartz crystals suggest their simultaneous formation. The presence of fluids with different density in syngenetic inclusions testifies to their entrapment in the course of phase separation of the initial fluid (entrapped in type 1 inclusions) during a drop of temperature and/or pressure (Fig.4). Since the fluid was situated on the two-phase equilibrium line during the entrapment, the measured homogenization temperatures correspond to the mineral formation temperatures. This inference is supported by data on the oxygen isotope thermometry (quartz–cassiterite pair). Pressure during the homogenization also matches the value during the entrapment of inclusions. For the H_2O–NaCl system, the pressure is 0.2 kbar at 400°C.

Based on the oxygen isotope data on quartz in granites and minerals in tin–tungsten ores, the ore-bearing fluids were likely derived from granites of the Badzhal batholith, given that the magmatogenic fluid came into the isotopic (and partly chemical) equilibrium with rocks at 500–550°C in the course of system evolution. The obtained factual data (lack of signs of the dilution and variations of $\delta^{18}O$‰ in the magmatogenic fluid) rule out any significant role of meteoric waters in the ore-forming system.

Table 3. Isotope abundance of oxygen of minerals and calculated values $\delta^{18}O$ aqueous phase in equilibrium fluid

№ sample	Mineral	$\delta^{18}O$ ‰(mineral)	T °C	$\delta^{18}O$ ‰ (H_2O)
Granites of Verkhne-Urmi massif				
BG-82	Quartz	11.2		
	Orthoclase	9.9	650	10.0 ± 0.2
BG-25	Quartz	11.0	500	8.5 ± 0.2
	Orthoclase	9.8		
Pravo-Urmi deposit. Cassitreite-topaz veinlets in greizens				
U-143-88	Topaz	8.2	450–550*	8.3 ±0.3
U-2-87	Topaz	9.1	380–480*	8.6 ±0.5
Blizhnee deposit. Quartz-cassiterite vein				
BSHU-1-14	Quartz	13.0	350–420	8.5 ±0.8
	Cassiterite	3.0		6.6 ±0.4

T *– upper limit of T mineral crystallization inclusive of probable influence of pressure on Tgom of inclusions. At calculation there are used equations from (Zheng 1993, Zhang et.al, 1994; Foure, Mensing, 2005)

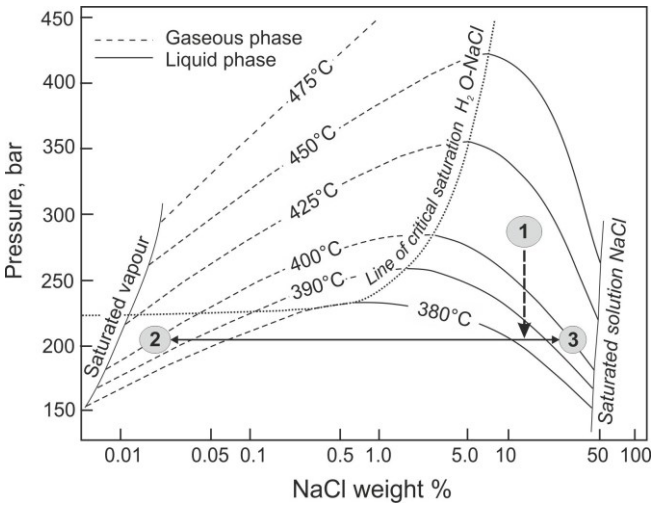

Fig. 4. PX-projection of isotherms at the system H_2O-NaCl (after Sourirajan, Kennedy, 1962), illustrating formation of the association of chloride brines and inclusions of vapour consenquence heterogenization of salt-water fluid with salinity 13 % NaCl during descent of temperature and pressure.

Isotope-geochemical research. According to the data from oxygen analysis in granite quartz and minerals of Sn-W ores, the probable source of ore-bearing of fluids could be granites of Badzhal batholitic pluton upon condition that magmatic fluid got into the isotope equilibrium (and very local chemical) with rocks at T=500-550°C under a process system evolution. Isotope abundance of oxygen of minerals of granites and Sn-W ores and lack of dilution marks and variations of $\delta^{18}O$ ‰ of magmatic fluid permits to conclude that ore-bearing fluids had magmatic origin. And therefore we cannot give significant role to meteoric waters at the ore-bearing system.

There is separated two-phase field of the coexistence of liquid and vapour (L+V) with index lines of salinity NaCl from 10 up to 70 wt. %, limited by lines of critical points (CP) and saturation line

(L+V+H) of solutions NaCl (Atkinson, 2002). Dotted line is – solidus of granite containing 2 wt. % F (Selby et al. 2000). There are noted depths corresponding to lithostatical (left axis) and hydrostatical grade. Greizen ores of Pravo-Urmi deposit formed at deep depth about 4-5 km at from the surface a high pressure whereas in contrast quartz-feldspar ores of Blizhnee one are generated near the surface at a low pressure, which determined heterogenization ore-bearing fluid (Fig.5).

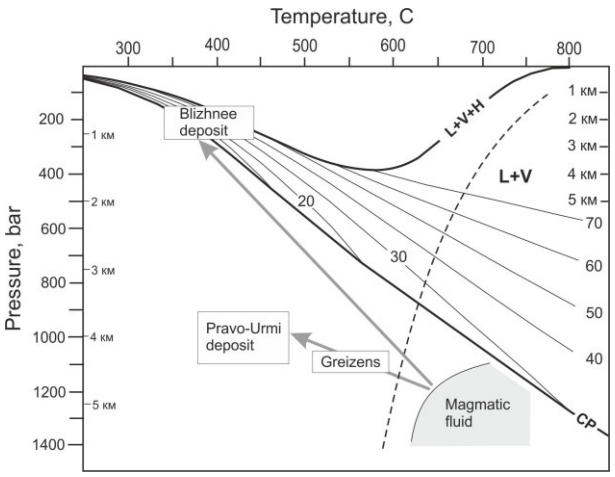

Fig. 5. The evolution pattern of Badzhal ore-magmatic system in PT-coordinates

Conclusions. Evidence from the conducted work we represented the evolution of tin-bearing Badzhal system and revealed formation conditions of two different deposits. Nature experiments are much complicated but they give more full picture of geological events and permit to reveal factors of ore formation. Nevertheless, experimental works improve certain moments of geological events. Therefore, it is instructive to connect something in between. Ore-bearing fluids in the Badzhal system were generated during the crystallization of felsic melts characterized by the moderate content of alumina, normal content of alkalis and elevated contents of H_2O (up to 8%), Cl (~0.1%) and F (~0.4%). The relatively dense (0.6 g/cm^3) supercritical water–salt fluid with a total salinity of 9–19% NaCl-equiv (0.72Na, 0.16K, 0.09Ca, 0.03Mg/0.93Cl, 0.07F) was fractionated at ~650°C and 1.2 kbar. Capacity of such fluid to transport a great number of components (As, B, Li, Rb, Cs, Sr, Zn, Cu and others) is indicated by both the data on water extracts and the presence of solid subsidiary phases in fluid inclusions.

Ores of the Pravo-Urmi deposit were formed during a decrease of the magmatogenic fluid temperature to ~500°C (greisenization) and 480–380°C (crystallization of cassiterite in the paragenetic association with topaz and quartz) accompanied by pressure fall from 1.2 to 1.0 kbar. At the total mineralization of 9–12 wt.% NaCl-equiv, the ore-forming solutions are characterized by the following proportions of the main salt components: (0.86Na, 0.1K, 0.03Ca, 0.01Mg/0.5Cl, 0.2F, 0.3HCO_3).

Cassiterite–quartz veins of the Blizhnee deposit were formed at 350–420°C from the water–salt solution of a similar composition (13 wt% NaCl-equiv; 0.92Na, 0.04K, 0.04Ca/0.5Cl, 0.5HCO_3) but in the course of its phase separation (heterogenization) owing to low pressure (0.2 kbar) during the mineral formation.

This work has done with funding from the programme of the Presidium RAS N 48 and Far East Division RAS (project № 15-I-2-003).

References:

Kryazhev S.G., Prokof'ev V.Yu., Vasyuta Yu. V.. Usage ICP MS method when analyzing the composition of ore-forming fluids from hydrothermal ore deposits//Vestnik of Moscow State University. 2006. Series 4. Geology. №4.. P .30-36.

Ognyanov N.V.Geology of tin-bearing districts and deposits of Khingan-Okhotsk tin province // Geologyof tin deposits SSSR. Nedra:1986. T.2. Volume 1. P. 280-340.In Russian.

Rodder E.. Fluid inclusions in minerals. Moscow:Mir. 1987. 560 p.

Rodionov S.M. Metallogeny of tin at Vostok of Russia. Moscow: Nauka. 2005. 327 p.In Russian.

Semenyak B.I., Rodionov S.M., Gonevchuk V.G. & al.. Tin-tungsten greizens грейзены, stockworks and quartz veins of Pravo-Urmi deposit//Geodynamics, magmatism and metalljgeny of Russian East. Edited by A.I.Khanchuk. Vladivostok: Dal'nauka. 2006. Volume.2. P. 611-619.In Russian.

Atkinson AB (A model for the PTX properties of H_2O-NaCl. Mc.Thesis, Virginia Tech. Institute and State Univ. 2002.

Foure G., Mensing T. Isotopes: principles and applications. /John Wiley & Sons, Inc., Hoboken, New Jersey. 2005. 897 p.

Selby D, Nesbitt BE, Muehlenbachs K Hydrothermal alteration and fluid chemistry of the Endako porphyry molybdenum deposit, British Columbia. Econ Geol 95:2000 P. 83-202.

Sourirajan S., Kennedy G.C. The system H_2O-NaCl at elevated temperatures and pressures// Amer. J. of Sci. V.260. 1962. P. 115-141.

Zhang, L.G., Liu, J.X., Chen, Z.S., Zhou, H.B., Experimental investigations of oxygen isotope fractionation in cassiterite and wolframite. Economic Geology, 1994.89, 150–157.

Zheng, Y.F., Calculation of oxygen isotope fractionation in hydroxyl-bearing silicates. Earth and Planetary Science Letters 120, 1993. 247– 263.

Ermina O.S.[1], Stennikov A.V.[1], Bychkov A.Yu.[1,2] Hydrothermal transformation of chlorella Sp. Biomass and the distribution of the elements between the aqueous solution and the hydrocarbon phase. UDC 550.4.02

[1] M.V. Lomonosov Moscow State University, Department of Geology, Russia, Moscow, (oermina6@yandex.ru) (ya_email@mail.ru) (andrewbychkov@rambler.ru).

[2] V.I. Vernadsky Institute of Geochemistry and Analytical Chemistry RAS, Russia, Moscow. 8-985-728-36-71, oermina6@yandex.ru.

Abstract. In recent years a lot of studies in regards to transformation of different types of algae into crude oil have been carried out. In our research experiments with biomass samples of Chlorella Sp. were conducted in titanium crucibles at 300°C and the pressure of saturated water vapor. Duration of experiments varied from 1 to 28 days. According to results, as the duration of the experiment increases, the quality of oil improves. Zn, Ni, Fe, Ca, K, S and Cu are distributed in oil. Biomass of algae Chlorella Sp. contains Zn, Fe, Ca, K and S. Thus Ni and Cu concentrate in oils from solution. Also the concentration of Ni rises along with increment of added Ni in solution.

Keywords: *Bio-oil; Algae; Chlorella Sp.; Elements, XRF; Ni.*

In recent years development of fields of non-conventional hydrocarbons is actively stepping up. A lot of research of transformation of various types of algae into oil has been carried out. Optimal temperature of hydrothermal treatment (Biswas et al., 2017), effects of added catalysts (Anastakis, Ross, 2011), increased oil output by risen heating rate (Bach et al., 2014) were studied, also oil production from different algae species and differences of output were investigated (Reddy et al., 2016). In these papers the possibility to obtain a mixture of hydrocarbons similar in composition to natural heavy oil or bitumen from algae biomass has been demonstrated. In this research organic composition of products was not studied in details. The mixture of hydrocarbons obtained from hydrothermal treatment of algae biomass in this paper is called "oil". Algae *Chlorella sp.* were used as precursor. This type of organic matter was chosen due to algae being a major source of organic compounds for oil formation in nature. *Chlorella sp.* is easily cultivated and thus readily available. Main objective of this research is to study peculiarities of oil production from biomass of algae *Chlorella sp.* using hydrothermal treatment and the distribution of elements in water-biomass-oil system. Experiments on hydrothermal treatment of algae *Chlorella sp.* were carried out. The effects of duration of treatment and solution composition on oil production were studied, also elemental analysis of algae and obtained oil was made. Total of 12 experiments were conducted, obtained oil from 8 of them was analyzed via X-ray fluorescence method using Niton FXL-950. All experiments were carried out in Experimental geochemistry lab of Faculty of geology of MSU. Samples undergone treatment at 300°C and water vapor pressure. These values were used in consideration of previous work (Bychkov et al., 2015) where parameters of maximum oil production by hydrothermal treatment of rocks were studied.

All experiments were conducted using 20 ml titanium crucibles. Aqueous solution and algae tablets were placed in crucibles. Then closed, they were put in preheated to 300°C furnace for a certain amount of time (1, 3, 7 and 28 days), after that they were taken out, cooled off and opened. To extract oil, 5 ml of hexane were poured into crucibles, and then their contents were washed off with distilled water. In separatory funnel, the organic layer with hexane was separated from the aqueous solution and dried at room temperature under a fume hood. After evaporation of hexane, the mass of oil was determined. After that, forty-fold volume of hexane was poured into the glasses with oil, then, after 24 hours, everything was filtered through a paper filter into the weighing bottles, and the rest was filled with chloroform and filtered into another weighing bottles. The extracts were then evaporated at room temperature under fume hood and the amounts of maltenes and asphaltenes were determined. A total of 3 series of experiments (4 experiments in each) on hydrothermal transformation of algae *Chlorella sp.* were conducted. The first series (C-1) was kinetic, the second (C-5) - with a multi-element standard solution for ICP: ICP-MS-68A-A, Solution A, and the third (C-6) - with an acidified solution of $NiCl_2$. The content of the elements was determined on the Niton FXL-950.

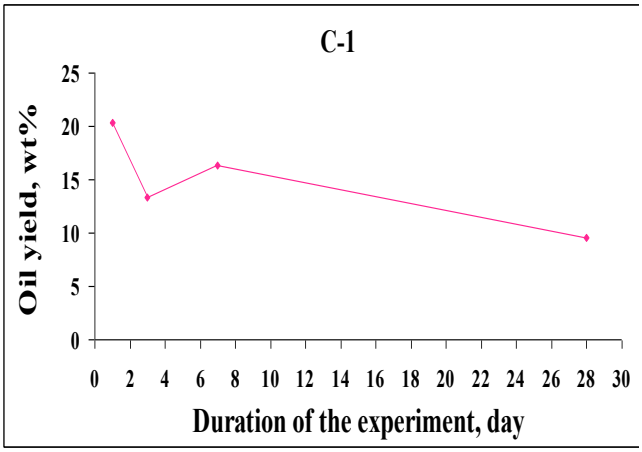

Fig.1. The diagram of oil yield, depending on the duration of the experiment in a series of experiments C-1.

Based on the results of the C-1 series, a diagram was constructed of the dependence of the oil yield on the duration of the experiment (Fig. 1) and the histogram of the ratio of maltens and asphaltenes, depending on the duration of the experiment (Fig. 2). The diagram (Fig. 1) clearly shows that the maximum yield of liquid hydrocarbons (20.3 wt.%) is observed in an experiment lasting for 1 day, and a minimum (9.5 wt.%) in an experiment lasting for 28 days. As shown on histogram (Fig. 2), the number of maltens increases and the amount of asphaltenes decreases as the experiment duration goes longer. Thus as the duration of experiment increases, the yield of oil decreases, but the quality of it improves, as the part of maltens rises. Presumably, maximum of oil yield is observed at day one, and this oil can be

called bitumen (as asphaltenes are predominant). Then, as the hydrothermal treatment goes on, the oil becomes more "light" due to the the decomposition of heavy hydrocarbons into lighter ones, as a result of which the amount of maltens increases and the amount of asphaltenes decreases. The results of the C-5 series showed that the longer the crucibles cool off, the less content of elements in oil. Elementalanalysis of the products showed that biomass of *Chlorella Sp.* contains Zn, Fe, Ca, K and S at concentrations above the detection limit. In oil, Zn, Fe, Ca, K and S, were found, as well as Ni and Cu which are not presented in *Chlorella Sp*. This means that Ni and Cu could be distributed into oil only from the solution, which means they are not inherited from the biomass of algae. All identified elements in oil and algae are biophilic. According to the results of experiments C-6, a graph of the Ni concentration after the experiment dependent on the concentration of Ni in oil was constructed (Fig. 3). It allows to say that on average, Ni between the solution and oil is distributed comparable: about half the amount of Ni that has been added to the solution is distributed into the oil. This experiment explains the accumulation of nickel in natural oils.

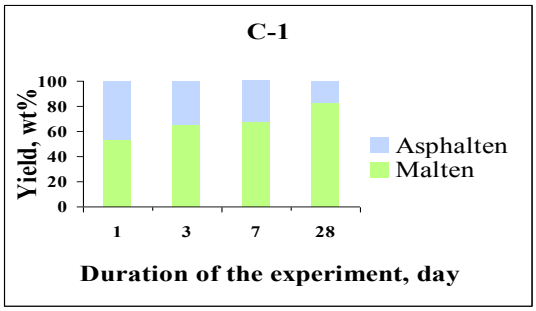

Fig. 2. Histogram of the ratio of maltens and asphaltenes depending on the duration of the experiment in a series of experiments C-1.

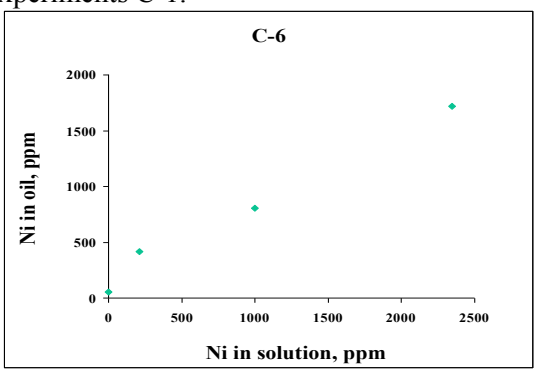

Fig. 3. Dependence of Ni concentration in oil after the experiment on concentration in aqueous solution.

The following peculiarities of formation of oil from algae were revealed. As the duration of the experiment increases, the yield of oil decreases, but its quality improves (the number of maltens increases).

Elemental analysis of oils showed that Zn, Ni, Fe, Ca, K, S and sometimes Cu are distributed into oil. Tablets of algae *Chlorella Sp.* contain Zn, Fe, Ca, K and S. Consequently, Ni and Cu are concentrated in the oils from the solution. The amount of Ni in the oils increases as the amount of Ni added in the solution increases.

Acknowledgments: The work was supported by the Russian Foundation for Basic Research, project 18-05-00818.

References:

Бычков А. Ю., Калмыков Г. А., Бугаев И. А., Козлова Е.В. Экспериментальные исследования получения углеводородных флюидов из пород баженовской свиты при гидротермальном воздействии // Вестник Московского университета. Серия 4: Геология. — 2015. — № 4. — С. 34-39

Anastasakis K., Ross A.B. Hydrothermal liquefaction of the brown macro-alga Laminaria Saccharina: Effect of reaction conditions on product distribution and composition // Bioresource Technology 102. — 2011. — P. 4876–4883

Bach Q.-V., Sillero M.V., Tran K.-Q., Skjermo J. Fast hydrothermal liquefaction of a Norwegian macro-alga: Screening tests // Algal Research. — 2014. — №6. — P. 271–276

Biswas B., Kumar A.A., Bisht Y., Singh R., Kumar J., Bhaskar T. Effects of temperature and solvent on hydrothermal liquefaction of Sargassum tenerrimum algae // Bioresource Technology. — 2017. №242.— P. 344-350

Reddy H.K., Muppaneni T., Ponnusamy S., Sudasinghe N., Pegallapati A., Selvaratnam T., Seger M., Dungan B., Nirmalakhandan N., Schaub T., Holguin F.O., Lammers P., Voorhies W., Deng S. Temperature effect on hydrothermal liquefaction of Nannochloropsis gaditana and Chlorella sp. // Applied Energy. — 2016. — №165. — P. 943–951

Korzhinskaya V.S. Effect of the fluid composition (Hf+HCl) on the behavior of Ta, Nb at dissolution of pyrochlore and tantalite at T=400, 500 and 550 °C, P=1000 bar (buffer Co-CoO)

Institute of Experimental Mineralogy, RAS Chernogolovka, Moscow district

Abstract. Experimental investigations of study of natural mineral solubility of pyrochlore $(Ca, Na)_2(Nb, Ta)_2O_6(O, OH, F)$ and tantalite $(Mn,Fe)_2(Nb,Ta)_2O_6$ in mixed fluids (HF+HCl) have been done. They allowed us to estimate equilibrium contents of metals of Ta and Nb in the solutions at T=400-550°C, P=1000 bar in the presence of oxygen buffer (Co-CoO). The runs have been done at a hydrothermal high pressure vessel in welded platinum tubes using capsule technique. Quenching solution has been analyzed by ICP/MS and ICP/AES (mass-spectral and atomic-emission) methods, but a solid charge has been analyzed by the x-ray-phase and microprobe analysis

methods. The initial concentration HF varied from 0.01 m to 2 m, but concentration HCl remained constant and was 0.5 m. A conclusion has been made that in (HF+HCl) solutions tantalite dissolves incongruently with a predominant transition into the solution Mn and Fe as compared with Ta and Nb. A comparison of Ta and Nb contents for pyrochlore and tantalite in equilibrium solutions has been made. The influence of concentration and temperature on solubility of these minerals has been determined.

Keywords: *experiment, pyrochlore, tantalite, solubility, mixed fluoride-chloride solutions, tantalum, niobium*

Investigations on solubility of natural minerals of tantalite-columbite $(Mn,Fe)_2(Nb,Ta)_2O_6$ and pyrochlore $(Ca, Na)_2(Nb, Ta)_2O_6(O, OH, F)$ in mixed fluids (HF+HCl) at T = 400, 500 and 550°C and P = 1000 bar in the presence of oxygen buffer Co-CoO are continued. Earlier we studied concentration dependence of solubility of these natural minerals at T = 550°C and P = 1000 bar (Korzhinskaya, 2017; Korzhinskaya, Kotova, 2017). Temperature dependence of behavior of Nb and Ta at dissolution of natural minerals of pyrochlore and tantalite for temperatures 400, 500 and 550°C and pressure 1000 bar has been studied in this paper. For the runs monocrystals of tantalite from quarz-amazonite-micaceous pegmatites of the Etykin tantalum deposit with the composition on microprobe data CamScan: Ta_2O_5 – 17.70; Nb_2O_5 – 58.99; MnO – 13.51; FeO – 4.42; TiO_2 – 2.59; SnO_2 – 1.54; WO_3 – 1.24 wt.% and pyrochlore monocrystals $(Ca,Na)_2(Nb,Ta)_2O_6(O,OH,F)$ from the weathering crusts of the deposit Tatarka of the following composition: Na_2O – 7.61; CaO – 14.28; Nb_2O_5 – 71.61; F – 5.18; TiO_2 – 0.83; $Ta_2O_5 \leq 1$ wt.% have been chosen. The initial concentration HF varied from 0.01m to 2m, but concentration HCl remained constant and was 0.5m. The runs were performed at a hydrothermal high pressure vessel in welded platinum tubes with the use of capsule technique. The quenching solution was analyzed by ICP/MS and ICP//AES methods (mass-spectral and atomic emission). Temperature dependence of the equilibrium content of Ta and Nb at tantalite dissolution in (HF+0.5mHCl) solutions is shown in Figs. 1 and 2. As Fig.1 shows at 400°C in the region of low concentrations (0.01-0.1m HF +0.5m HCl) the equilibrium content of Ta is by 2.5-2 orders of magnitude lower than that at 550°C and is only $n \cdot 10^{-8}$ mol/kg H_2O. The similar picture is also observed for Nb in the region of low concentrations. As the concentration of HF increases, the content of niobium and tantalum increases sharply by 3.5-4 orders of magnitude in the region of high concentrations of HF (1m HF + 0.5m HCl) and (2m HF + 0.5m HCl) and reaches $n \cdot 10^{-3.5}$ mol/kg H_2O. The contents of Mn and Fe in mixed (HF + 0.5m HCl) solutions for tantalite are much higher than for niobium and tantalum (Korzhinskaya, 2017).

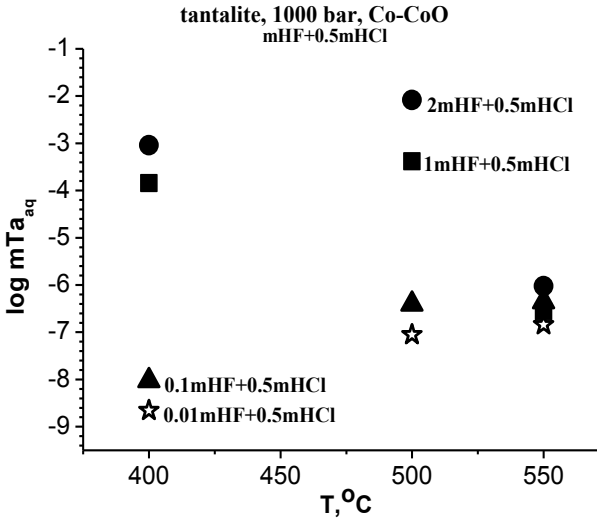

Fig.1. Temperature dependence of equilibrium content of Ta in (HF+HCl) fluids at dissolution of natural tantalite at T=400, 500 and 550°C, P=1000 bar (buffer Co-CoO).

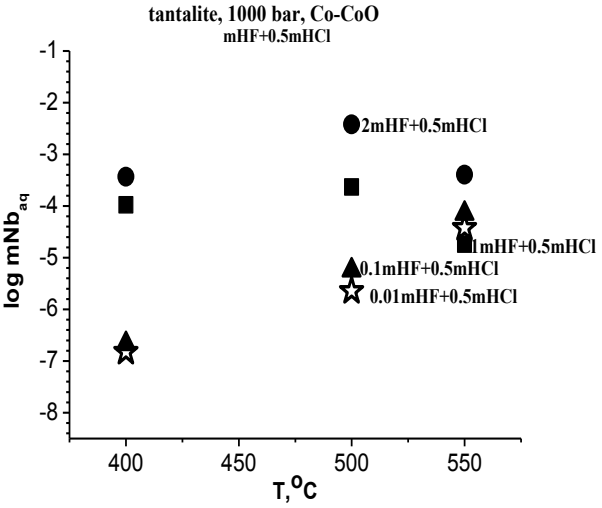

Fig.2. Temperature dependence of Nb equilibrium content in ((HF+HCl) fluids at dissolution of natural tantalite at T=400, 500°C, P=1000 bar (buffer Co-CoO).

In (0.01m HF+0.5m HCl) the equilibrium content of Mn is $3.93 \cdot 10^{-3}$, but that of Fe is $7.70 \cdot 10^{-4}$ mol/kg H_2O at 550°C and P = 1000 bar. In the region of high concentrations HF the contents of Mn for T = 400 and 550°C are comparable and are n 10 mol/kg H_2O. The content of Fe for 400 °C remains practically constant. It is determined that for T = 400°C concentration dependence both for Ta and Nb has a more marked linear dependence than for 550°C. The similar picture was also seen in chloride solutions where the content of Mn and Fe for all chloride solutions is rather higher than that of Ta and Nb (Korzhinskaya, 2014). So, both for pure chloride solutions and mixed ones (HF+HCl) natural tantalite dissolves sharply incongruently with the predominant transition into the solution of Mn and Fe as compared with Ta and Nb.

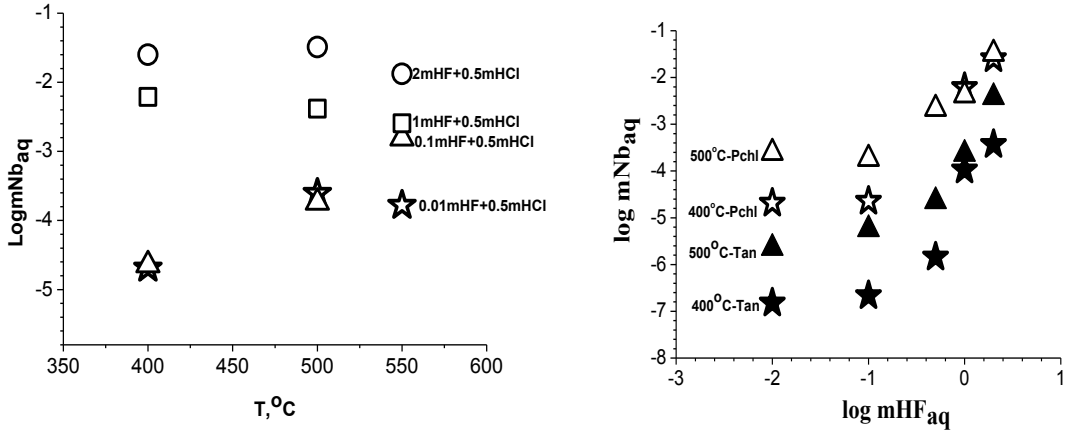

Fig.3. Temperature dependence of equilibrium Nb content in the solutions at pyrochlore dissolution (T=400°, 500°C, P=1000 bar).
Fig.4. Concentration dependence of equilibrium Nb content in the solutions at pyrochlore and tantalite dissolution (T=400°, 500°C, P=1000 bar), (non-painted figures-pyrochlore; colored – tantalite).

Fig. 3 represents temperature dependence of equilibrium Nb content at pyrochlore dissolution. In the region of low concentrations (0.01m HF+0.5m HCl) and (0.1m HF + 0.5m HCl) temperature dependence has a practically linear character: as temperature rises Nb content in the solution increases . The content of Nb in the solution rises markedly as HF concentration grows: for 400°C in (0.1m HF+0.5m HCl) Nb content is $2.26\cdot10^{-5}$ mol/kg H_20 but for (2m HF +0.5m HCl) it is $2.52\cdot10^{-2}$ mol/kg H_20. For 500°C, this dependence is 1-1.5 orders of magnitude: for diluted solutions Nb content in the solution is $1.83\cdot10^{-4}$, but in concentrated solutions it is $n\cdot10^{-2}$ mol/kg H_20. For more concentrated solutions HF temperature dependence has a reverse character: as temperature grows inconsiderably (only by an order of 0.5) Nb content in the equilibrium solution decreases. Form comparison Fig.4 shows concentration dependences of Nb content at dissolution of pyrochlore and tantalite for two temperatures: 400° and 500°C and P = 1000 bar.

We can see that for both temperatures Nb content at pyrochlore dissolution for all concentrations HF is considerably higher than at tantalite dissolution by more than 2 orders in the region of low concentrations. For concentrated solutions (1-2m HF +0.5m HCl) this difference is only of an order of 1-1.5. However, it is pointed out that pyrochlore solubility is considerably higher in (HF+HCl) solutions than tantalite solubility where Mn and Fe transfer in to the solution more preferably than Ta and Nb.

It was confirmed by these experiments that at such low contents of Ta close to the limit of discovery it is difficult to make conclusions about the influence of Cl-ion on tantalite solubility and, consequently, about any marked role of complexation of tantal with Cl under natural conditions.

The experimental data obtained by us make it possible to confirm that the experimentally determined fact is principally important to understand the genesis of Ta and Nb deposits. The idea of this fact is that a hydrothermal transport of metals of Ta and Nb in the amounts necessary to form their industrial concentrations is possible only by fluorine solutions.

This work was supported by the ONZ RAS program and grants of RFBR 15-05-03393-a

References:

Korzhinskaya V.S. The effect of fluid composition (HF+HCl) on the behavior of metals (Ta, Nb, Mn, Fe) at tantalite dissolution at T=550°C, P=1000 bar (buffer Co-CoO) // In: Proceeding of Russian Annual Seminar of Experimental Mineralogy, Petrology and Geochemistry (RASEMPG-2017), Moscow, 18–19 April 2017, p.p. 120-121.

Korzhinskaya V.S., Kotova N.P. The behavior of oxides of Nb and Ta, pyrochlor and tantalite in mixed aqueous solutions (HF+HCl) at T=550°C and P=1000 bar. // In: Proceeding of Russian Annual Seminar of Experimental Mineralogy, Petrology and Geochemistry (RASEMPG-2017), Moscow, 18–19 April 2017, p.p. 122-123.

Korzhinskaya V.S. The effect of fluid composition on the behavior of Mn and Fe at solubility of columbite – tantalite. // Experimental Geochemistry, 2014.V.2, N3. Pp. 309-313.

Kotelnikov A.R.[1], Suk N.I.[1], Akhmedzhanova G.M.[1], Kotelnikova Z.A.[2], Gramenitskiy E.N.[3], Schekina T.I.[3], Polskoy P.F.[1] Fluorine and chlorine distribution between sodalite and hydrothermal fluid. UDC 549.057, 548.736.6

[1]Institute of Experimental Mineralogy RAS, Chernogolovka Moscow district,
[2]*Institute of Geology of Ore Deposits, Petrography, Mineralogy, and Geochemistry, RAS, Moscow, Moscow State University of M.V. Lomonosov, geology district, Moscow*
(kotelnik@iem.ac.ru, sukni@iem.ac.ru, kotelnik@igem.ru)

Abstract. Fluorine and chlorine distribution between sodalite and hydrothermal fluid has been experimentally investigated at 650°C and 2 kbar used autoclave

equipment, hydrothermal vessel and high gas pressure vessel. It has been shown that solid solutions of F,Cl-bearing sodalites are characterized by wide immiscible field. Based on these data the values of excess mixing functions of the solid solution (F, Cl)-sodalites were calculated. The distribution of fluorine and chlorine in the sodalite – fluid system is not ideal, alternating. At $X_F^{fl} \leq 0.75$, fluorine enriches the fluid with respect to the sodalite, and at $X_F^{fl} > 0.8$ fluorine begins to enrich the sodalite (T = 650 °C, P = 2 kbar).

Keywords: *experiment, sodalite, hydrothermal fluid, fluorine, chlorine, solid solution*

Sodalite is sufficient widespread mineral of alkaline complexes. Total formula of sodalites (minerals of framework aluminosilicate group) – $Na_8Al_6Si_6O_{24}(X)$, where X – such anions as Cl^-, Br^-, I^-, SO_4^{2-}; CO_3^{2-}; OH^- and others. As a rule, sodalites crystallize in cubic crystal system, space group P43m. In addition to anionic isomorphism, they are characterized by substitutions in the position of an alkaline cation: sodium in small amounts can be replaced by potassium and calcium. Sodalites are common in alkaline magmatic rocks, sometimes found in pegmatites.

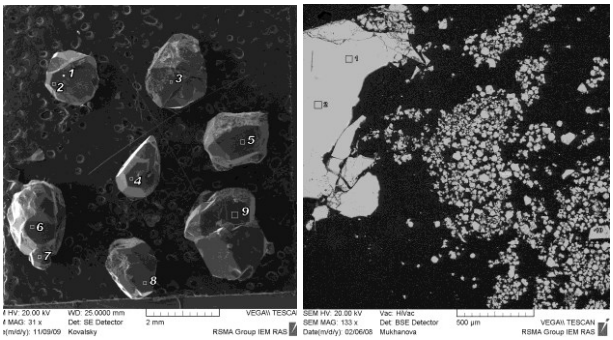

Fig. 1. Pure fluoride-sodalite synthesized at 650°C, 2 kbar.

Earlier at 650°C, 2 kbar, we have synthesized pure fluorine-sodalite (Fig. 1). The crystal structure of the F-sodalite was determined by O.V. Yakubovich et al. (2011) (diffractometer: Xcalibur-S-CCD; $2\Theta max = 64.99°$; R = 0.037 for 440 reflexes). The disordered framework of Al, Si tetrahedrons is topologically identical to the framework of natural sodalites. Na^+-cations, $[AlF_6]^{3-}$-anions and water molecules are located in the cavities of the sodalite structure (Fig. 2). According to the structural study and microprobe analysis, the following formula for F-containing sodalite is proposed (Yakubovich et al., 2011): $Na_{7.38}(AlF_6)_{0.70}(H_2O)_{4.88}[(Si_{6.74}Al_{5.26})O_{24}]$. Cell parameter a=9.0461(1); space group P4(-)3m; Z=1; ρ(calculated)= 2.370 g/cm^3.

The question arose: does F-containing sodalite occur in natural parageneses? I.V. Pekov kindly had provided us with a sample of the sodalite rock with villiomite phenocrysts, in which fluorine-containing sodalite was found as a solid solution (F, S, Cl)-sodalite. The average composition of (F, S, Cl)-sodalite (wt%): SiO_2 – 33.65(45); Al_2O_3 – 29.10(42); Na_2O – 23.96(59); F – 0.92(12); SO_3 – 4.48(13); Cl – 4.91(27).

In this connection, the task was to synthesize a solid solution of (F, Cl)-sodalite and study the distribution of fluorine and chlorine between sodalite and fluid.

Experimental method. The experiments were carried out using autoclaves, hydrothermal devices with the external heating and cold valve and high gas pressure vessel at 650°C and 2 kbar by ampoule method using platinum and gold ampoules. Duration of experiments was from 15 up to 25 days. As starting materials $NaAlSiO_4$ gel, distilled water and salts NaF and NaCl were used. We have added 1 wt% of "seeding" natural chlorine-sodalite to the charge. The initial compositions of the experiments are presented in Table 1. The solid products of the experiments were studied by microprobe and X-ray analysis; the composition of the fluids after the experiments was studied by atomic absorption analysis and ion-selective potentiometry.

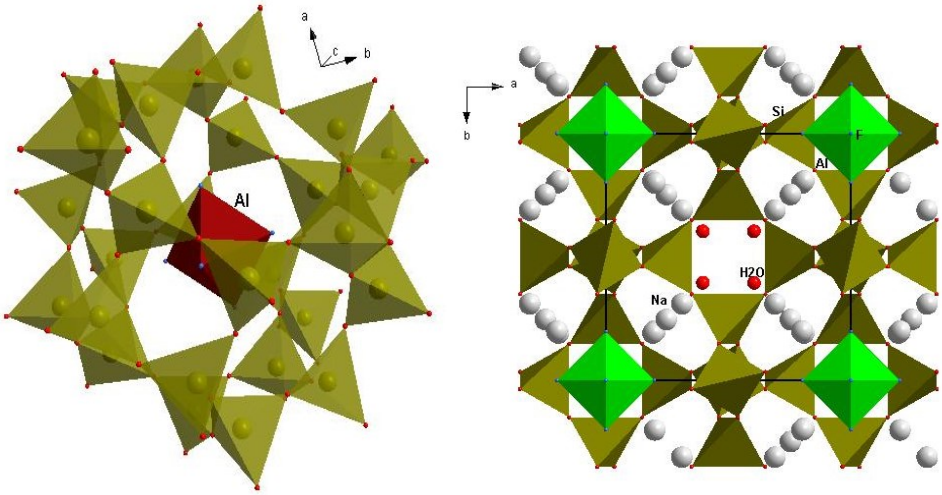

Fig. 2. Crystal structure of F-sodalite (Yakubovich et al., 2011).

Table 1. Initial materials and results of experiments on the study of isomorphic substitutions (F↔Cl) in sodalites at T=650°C and P=2 kbar.

Before experiments				After experiments	
NaF, mg	NaCl, mg	H_2O, mg	X_F^{fl}	Experiment products	X_F^{Sod}
15.2	84.7	100	0.20	Cl-Sod +Can +L	0.05
41	58	100	0.50	Cl-Sod+Cry+L	0.055
70	33.5	104	0.74	Cl-Sod+F-Sod+ Cry+L	0.045÷0.92
37.5	2.5	60	0.95	Cl-Sod+F-Sod+ Cry+L	0.13÷0.97
35.5	1.5	60	0.97	F-Sod+Can	0.98
75	0	75	1	F-Sod + Ab	1
19	56	75	0.32	Cl-Sod + Ab	0.05
38	38	75	0.58	Cl-Sod+F-Sod +L	0.06 ÷ 0.94
56	19	75	0.80	Cl-Sod+F-Sod	0.05 ÷ 0.89
67	8	75	0.92	F-Sod	0.94
8	67	75	0.14	Cl-Sod	0.03

Notice. Cl-Sod – chlorine-sodalite, F-Sod – fluorine-sodalite, Cry – cryolite, L – melt, Can – cancrinite, Ab – albite.

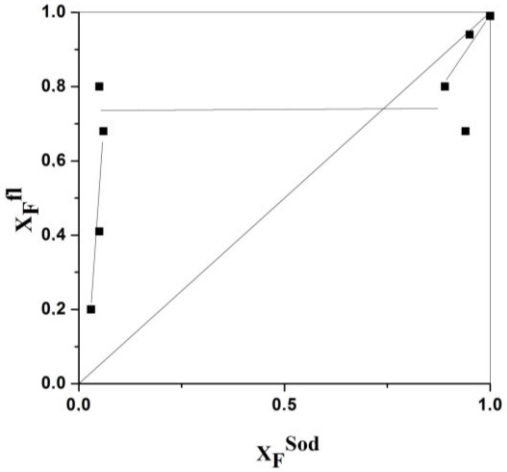

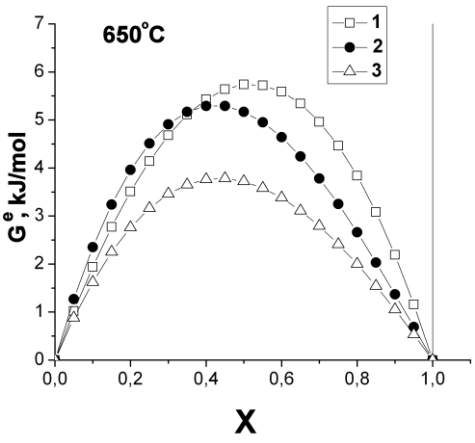

Fig. 3. Distribution of fluorine and chlorine between sodalite and fluid at 650°C and 2 kbar.
Fig. 4. Excess mixing energies for (F, Cl) -; (Cl, SO_4) - sodalites and (Na, K) - feldspars, calculated on the basis of compositions of coexisting phases. 1 – (F, Cl)-Sod; 2 – (Cl, SO_4)-Sod; 3 – (Na,K)-Fsp .

Experimental results. Results of experiments are presented in Table 1. Experimental results have shown that solid solutions of (F,Cl)-bearing sodalites are characterized by a wide immiscibility field. Distribution of fluorine and chlorine in the system sodalite – fluid is non-ideal, alternating (fig. 3). At $X_F^{fl} \leq 0.75$ fluorine enriches the fluid concerning sodalite, and at $X_F^{fl} > 0.8$ fluorine begins to enrich the sodalite (T = 650°C, P = 2 kbar). To generate fluorine-sodalite, high values of the mole fraction of fluorine in the fluid are needed.

Based on the data on the boundaries of the immiscibility field, the values of the excess mixing functions of the solid solution (F, Cl)-sodalites were calculated (Fig. 4).

Conclusions

1. Solid solutions of (F, Cl)-sodalites have been synthesized in hydrothermal conditions (T=650°C; P=2 kbar). Boundaries of the immiscibility field of solid solution X_F^{Sod}=0.07÷0.93 are shown.

2. The distribution of fluorine and chlorine between a solid solution of (F, Cl)-sodalites and an equilibrium hydrothermal fluid was studied.

3. Excess mixing energies of solid solutions (F, Cl)-sodalites are calculated.

Reference:

Yakubovich O.V., Kotelnikov A.R., Schekina T.I., Gramenitskiy E.N., Zubkov E.S. New representative in the structural type of sodalite with non-framework anions $[AlF_6]^{3-}$. Krystallografiya. 2011. V. 56. N 2. P. 217-224.

Kotova N.P. Experimental study of temperature influence on niobium oxide solubility in chloride HCl and KCl solutions.

Institute of Experimental Mineralogy RAS, Chernogolovka, Moscow district (kotova@iem.ac.ru)

Abstract. The dependence of Nb_2O_5 solubility as a function of temperature was investigated in HCl and KCl solutions with concentrations 0.1 and 1 m at 300 and 500°C and 100 MPa under Co-CoO oxidizing conditions. It was found that in chloride solutions of different cationic composition (HCl and KCl), the temperature dependence of the solubility of Nb_2O_5 in the temperature range 300-

550°C, P = 100 MPa, (Co-CoO buffer) is weakly expressed. The solubility of niobium is low and ranges from 10^{-5} to 10^{-4} m.

Keywords: *experiment, oxide niobium, hydrothermal solubility, temperature, chloride solutions*

To model the conditions of the tantalum deposits formation, in addition to the magmatic factor, it is also necessary to take into account the role of hydrothermal-metasomatic processes. Therefore, we carried out experimental studies of the behavior of rare metals in aqueous fluids at temperatures and pressures that correspond to the physicochemical parameters of postmagmatic processes, aimed at obtaining quantitative estimation of the physicochemical conditions for the formation of greisenized and albitized W, Mo, Sn, Ta, Nb and Li deposits, associated with standard calc-alkaline, including lithium-fluoride granites.

New experimental data on the solubility of niobium oxide (Nb_2O_5), an analog of the natural mineral nioboxide, were obtained in aqueous chloride solutions consisting of 0.1 and 1.0 m HCl and KCl at 300 and 500°C and 100 MPa under Co-CoO oxidizing conditions. The run duration was 30 days at 300 and 21 days at 500°C. Experiments were performed on a hydrothermal line. A sealed-capsule quench technique was employed. The same technique was used to study Ta_2O_5 and Nb_2O_5 solubility in fluoride solutions.

The quenched aqueous solutions were then analyzed using ICP/MS (Inductively Coupled Plasma Mass Spectrometry) and ICP/AES (Atomic Emission Spectroscopy) for Nb, Ta, Mn, and Fe and admixture elements Ti, W, and Sn,.

To control congruent or incongruent dissolution of Nb oxide and to determine chemical composition of newly-formed phases (in case of their detection) the initial materials and solid run products were studied by X-ray diffraction, and electron microprobe analysis (Cam Scan MV 2300 (VEGA TS5130MM).

Experimental data on Nb_2O_5 solubility at 300 and 500°C, P = 100 MPa, and also the previously obtained data on the solubility of Nb_2O_5 at 400 and 550°C, P = 100 MPa are shown in Fig. 1 (Kotova, 2015). Studies have shown that the equilibrium content of niobium in 0.1 and 1 m HCl solutions at 300°C practically have the same value ($10^{-5.7}$ mol/kg H_2O). When the temperature rises from 300°C to 550°C, the niobium content in 0.1 m HCl solution slightly increases from $10^{-5.7}$ mol/kg H_2O to $10^{-5.3}$ mol/kg H_2O, remaining at the same low level. In solutions of 1 m HCl with an increase in temperature from 300 to 550°C, the equilibrium content of niobium increases by approximately 1.5 orders of magnitude - from $10^{-5.7}$ mol/kg H_2O to $10^{-3.9}$ mol/kg H_2O.

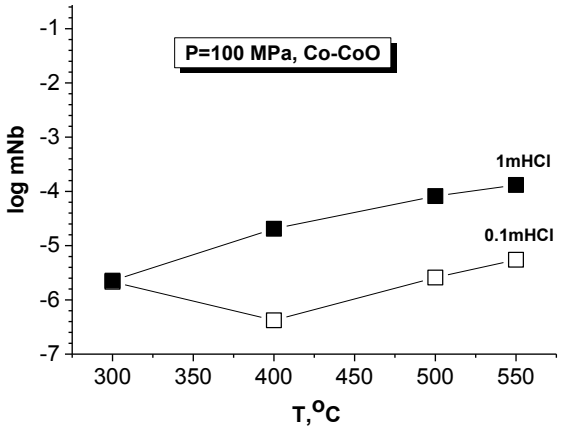

Fig. 1. Temperature dependence of Nb_2O_5 solubility in HCl solutions at P = 100 MPa (Co-CoO buffer)

Experimental data on the solubility of Nb_2O_5 in 0, 1 and 1m KCl solutions at 300 and 550°C and P = 100MPa as a function of temperature are shown in Fig. 1 (Kotova and Korzhinskaya, 2015). Analysis of experimental results on the solubility of niobium oxide in solutions of 0.1 and 1 m KCl showed that the trends of temperature dependence of niobium oxide solubility are similar. With an increase in temperature from 300 to 550°C, the equilibrium content of niobium in solutions of 0.1 and 1 m KCl practically does not change, remaining at the level of 10^{-5} mol/kg H_2O.

The data of X-ray diffraction of solid run products clearly show that, for the range of concentration of HCl and KCl solutions and temperatures considered in this study, at P = 100 MPa, niobium oxide dissolves congruently, that is, without changing its composition.

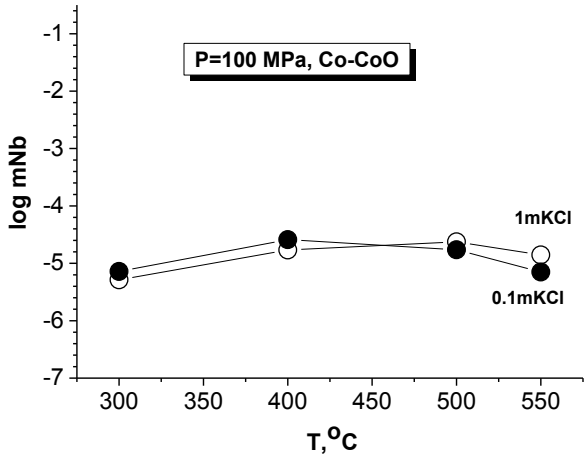

Fig. 2. Temperature dependence of Nb_2O_5 solubility in KCl solutions at P = 100 MPa (Co-CoO buffer)

It was found that in chloride solutions of different cationic composition (HCl and KCl), the temperature dependence of the solubility of Nb_2O_5 in the temperature range 300-550°C, P = 100 MPa, (Co-CoO buffer) is weakly expressed. The solubility of niobium is low and ranges from 10^{-5} to 10^{-4} m.

At such low concentrations, it is difficult to judge the real mass transfer of niobium by chloride hydrothermal solutions and the possibility of the formation of its commercially viable ore deposits.

This work was supported by the grants of RFBR 18-05-01001-a

References:

Kotova N.P. Experimental study of the solubility of Nb_2O_5 in chloride solutions at T = 300 and 550°C and P = 100 MPa. Proceedings of the All-Russian Annual Seminar on Experimental Mineralogy, Petrology and Geochemistry. Moscow, April 21-22, 2015 in 2 volumes. Otv. editor A. A. Kadik, - M: GEOKHI RAS, p.147

Kotova N.P., Korzhinskaya V.S. Experimental study of the behavior of niobium oxide and natural pyrochlore in fluoride and chloride solutions // In: XVII All-Russian Conference on Experimental Mineralogy. Section III-Phase equilibrium in silicate and ore systems. Novosibirsk, 2015, p.92.

Kotova N.P. Experimental study of effect of fluid (HF + HCl) composition on the solubility of tantal oxide at T =400-500°C, P = 100 MPa.

Institute of Experimental Mineralogy RAS, Chernogolovka Moscow district (kotova@iem.ac.ru)

Abstract. New data on the solubility of tantalum oxide in mixed (HF + HCl) fluids at T = 400 -500°C and P = 100 MPa in the presence of the oxygen buffer Co-CoO are obtained. The initial HF concentration varied from 0.01m to 2m, and HCl concentration remained constant and was 0.5 m. The limiting contents of tantalum in hydrothermal fluids of different composition are determined and the comparative characteristics of Ta's behavior depending on the concentration and composition of the solution are obtained. It is found that the dependence of the solubility of tantalum oxide on temperature in mixed fluoride-chloride solutions is practically absent. In the region of low initial concentrations of solutions (0.01 m HF + 0.5 m HCl) the equilibrium concentration of Ta is only 10^{-7} mol/kg H_2O, and in the region of high fluid concentrations (2 m HF + 0.5 m HCl) it increases to 10^{-2} mol/kg H_2O,

***Keywords**: experiment, oxide tantalum, hydrothermal solubility, fluoride-chloride solutions*

Experimental studies of the behavior of Ta during the dissolution of tantalum oxide in solutions of mixed composition (HF + HCl) at T = 400-500°C, P = 100MPa (Co-CoO buffer) were carried. The initial HF concentration varied from 0.01m to 2m, and HCl concentration remained constant and was 0.5 m. Experiments were performed on a hydrothermal line. A sealed-capsule quench technique was employed. After the run the quenched aqueous solutions were analyzed using ICP/MS (Inductively Coupled Plasma Mass Spectrometry) and ICP/AES (Atomic Emission Spectroscopy) for Nb, Ta, Mn, and Fe and admixture elements Ti, W, and Sn. The composition of the solid run products was characterized using optical microscopy, X-ray diffraction, and electron microprobe analysis (Cam Scan MV 2300 (VEGA TS5130MM.

The limiting contents (solubility) of tantalum in hydrothermal fluids of various compositions were determined and the comparative characteristics of the tantalum behavior were obtained as a function of the concentration and composition of the solution at T = 400, 500, and 550°C, 100 MPa (Fig. 1, 2, 3, and 4).

The results of the experiments presented in Fig. 1 showed that the trends of the dependence of Ta_2O_5 solubility on temperature in complex fluids (HF + HCl) of different concentrations at T = 400, 500, and 550°C, P = 100 MPa (Co-CoO buffer) are almost identical. It has been established that in the region of low initial concentrations of the F - ion (0.01mHF + 0.5mHCl), the equilibrium concentration of Ta at T = 400 and 500°C is only 10^{-7} mol/kg H_2O, and at T = 550°C – 10^{-6} mol/kg H_2O. At high F^- ion concentrations (2 m HF + 0.5 m HCl), the equilibrium concentration of Ta increases to 10^{-2} mole/kg H_2O, that allows us to state that at the studied temperatures and P = 100MPa the dependence of tantalum solubility on F - ion concentration in mixed fluids has a clearly expressed positive character.

For comparison, the trends of tantalum oxide solubility in mixed fluoride-chloride and pure fluoride solutions as a function of temperature are shown in Fig. 2, 3 and 4 (Kotova, 2017, Korzhinskaya and Kotova, 2017). Analysis of the experimental results on the tantalum oxide solubility in fluoride and mixed fluoride-chloride solutions in the investigated temperature range 400-550°C and P = 100 MPa showed that the addition of Cl^- ion in the form of 0.5 m HCl to fluoride solutions of low concentration (0.1 m HF) reduces the solubility of tantalum oxide by about 1.5 orders of magnitude, and at high F- ion concentrations (1-2 m HF) the solubility of tantalum decreases by about 1 order. The temperature dependence of tantalum oxide solubility in mixed fluoride-chloride solutions is practically absent.

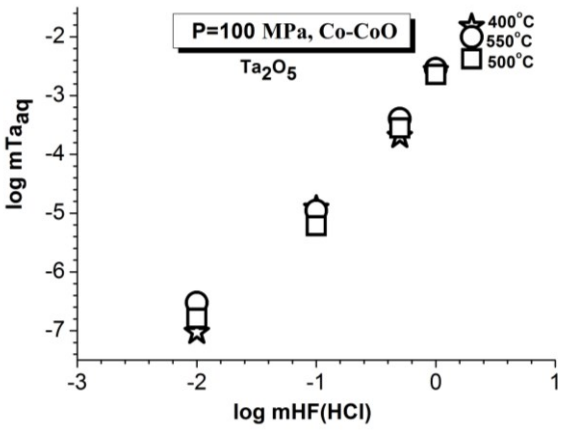

Fig. 1. Concentration dependence of tantalum content in mixed (HF + HCl) fluids during of tantalum oxide dissolution at T = 400, 500, and 550 ° C, P = 100 MPa (Co-CoO buffer)

For comparison, the trends of tantalum oxide solubility in mixed fluoride-chloride and pure fluoride solutions as a function of temperature are shown in Fig. 2, 3 and 4 (Kotova, 2017, Korzhinskaya and Kotova, 2017). Analysis of the experimental results on tantalum oxide solubility in fluoride and mixed fluoride-chloride solutions in the investigated temperature range of 400-550°C and P = 100 MPa showed that the addition of Cl - ion in the form of 0.5 m HCl to fluoride solutions of low concentration (0.1 m HF) reduces the solubility of tantalum oxide by about 1.5 orders of magnitude, and at high F- ion concentrations (1-2 m HF) the solubility of tantalum decreases by about 1 order. The temperature dependence of tantalum oxide solubility in mixed fluoride-chloride solutions is practically absent.

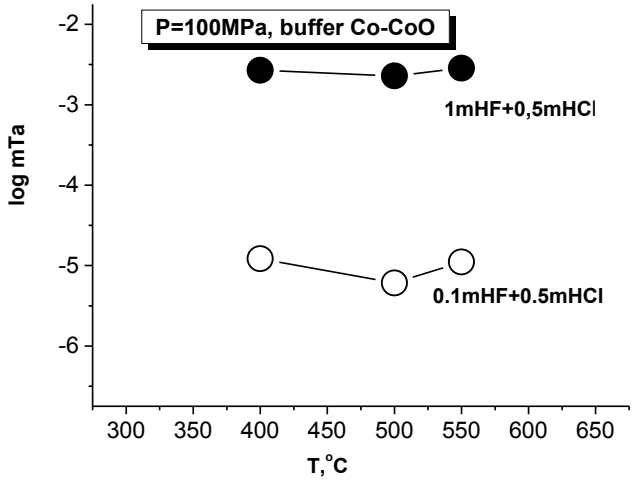

Fig. 2. Temperature dependence of Ta_2O_5 solubility in (0.1 m HF + 0.5 m HCl) and (1 m HF + 0. m HCl) solutions at P = 100 MPa (Co-CoO buffer)

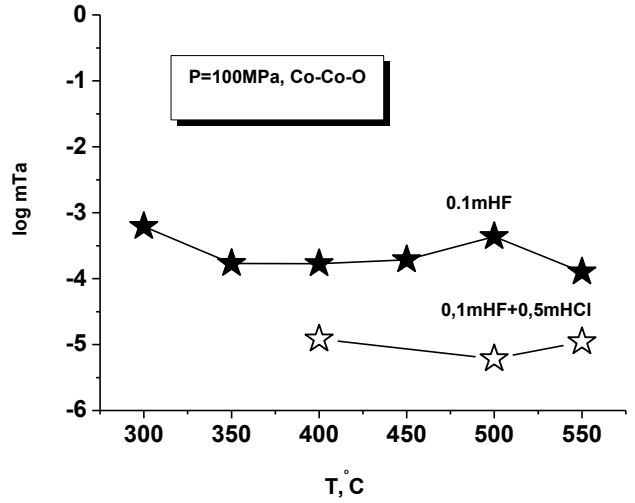

Fig.3. Temperature dependence of Ta_2O_5 solubility in 0.1 m HF и (0.1 m HF + 0.5 m HCl) solutions at P = 100 MPa (Co-CoO buffer)

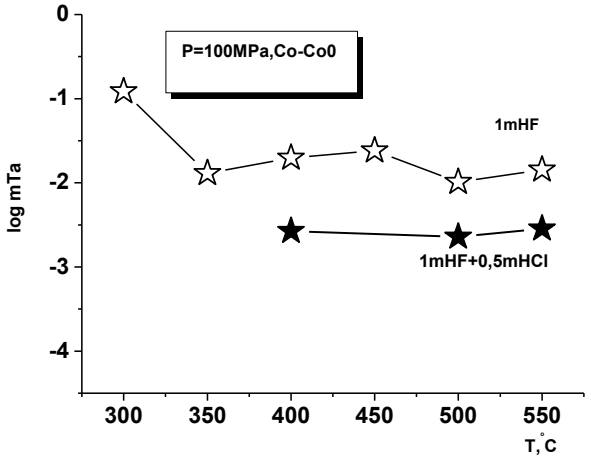

Fig.4. Temperature dependence of Ta_2O_5 solubility in 1 m HF и (1 m HF + 0.5 m HCl) solutions at P = 100 MPa (Co-CoO buffer)

Experimental studies on the solubility of Ta_2O_5 in mixed fluids (0.01-2m HF + 0.5m HCl) at T = 400-550°C and P = 100 MPa (Co-CoO buffer) showed that only concentrated fluoride and fluorine-containing solutions can dissolve the compounds of Ta and Nb and transport these elements in high-temperature hydrothermal conditions.

This work was supported by the grants of RFBR N 18-05-01001-a

References:

Kotova N.P. Experimental study of the influence of the fluid composition (HF + HCl) on the solubility of tantalum oxide at T = 550°C, P = 100 MPa // In: Proceedings of the All-Russian Annual Seminar on Experimental Mineralogy, Petrology and Geochemistry (WECEMPG-2017). Otv. Ed. O. A. Lukanin. Moscow, April 18-19, 2017 Moscow. GEOKHI RAS. 2017. p. 132-133. ISBN 978-5-905049-16-3.

Korzhinskaya VS, Kotova N.P. Behavior of oxides of niobium and tantalum, pyrochlore and tantalite in mixed aqueous solutions (HF + HCl) at T = 550°C and P = 1000 bar // In: Proceedings of the All-Russian Annual Seminar on Experimental Mineralogy, Petrology and Geochemistry (WECEMPG-2017). Otv. Ed. O.A. Lukanin. Moscow, April 18-19, 2017 Moscow. GEOKHI RAS. 2017. p. 122-123. ISBN 978-5-905049-16-3.

Lakshtanov[1,2] L.Z.', Okhrimenko[2] D.V., Karaseva[1] O.N., Stipp[2] S.L.S. Surface reactivity of chalks

[1] D.S. Korzhinskii Institute of Experimental Mineralogy RAS, Chernogolovka, Russia (leonid@iem.ac.ru),
[2] Nano-Science Center, Department of Chemistry, University of Copenhagen

Abstract. We studied the rates of calcite precipitation on the surface of the particles in various North Sea chalk samples, using the constant composition method for supersaturation states ranging from 2.4 to 4.5, at pH = 8.5. The rates of calcite precipitation on the chalk surfaces are much lower than on pure calcite surfaces. The

dependence of calcite precipitation rate on supersaturation does not obey the parabolic law, which is characteristic for calcite growth. Instead, the dependence was exponential, which indicates surface nucleation mediated growth. To gain better understanding about the interactions that occur at the chalk surface we determined the ζ - potential for the chalk samples. Our results show that the specific adsorption is the main reason for strong inhibition of calcite precipitation by the polysaccharides and certain other organic compounds. So, the presence of organic compounds has an important influence on recrystallization kinetics so along with other possible causes of inhibition, the mechanism of calcite precipitation is a factor in the extremely low rates of the chalk recrystallization.

Keywords: *calcite; chalk; precipitation; growth rate; surface nucleation; inhibition; polysaccharides; streaming potential*

It is well known that in a pure system calcite recrystallizes rapidly, increasing its crystal diameter dramatically, on the scale of days to months. Natural chalks, formed by sedimentation of coccoliths, the mineralized parts of the unicellular algae, behave quite differently. In many chalk samples, the original calcite coccoliths are very well preserved as intact or fragmented disks and individual elements, with sizes ranging from 0.5 to 10 μm, implying that recrystallization during diagenesis was minimal or negligible. This results in high porosity of chalks, a consequence of the lack of pronounced recrystallization and cementation (Fabricius et al., 2007).

The aim of this work was to understand the inhibitory effects of organic compounds on calcite and at the same time, to elucidate the reasons for the extremely low recrystallization rate of chalk.

Chalk samples were of Maastrichtian age and provided by Maersk Oil and Gas A/S, except for Ålborg chalk, which was collected from the Ålborg Portland quarry near Ålborg, Denmark. The Maersk Oil chalks were fragments from core samples drilled from a variety of locations in water saturated (2-3, 2-4, and 7-1) and gas saturated (10-4) zones in the Danish North Sea fields. Grain size was typically 0.5 - 5 μm.

With the constant composition method (pH-stat titration system) that was described earlier (e.g. Lakshtanov et al., 2011; Montanari et al., 2016), we investigated calcite precipitation on samples of natural chalks. The experiments were run thermostatically at 25°C in a double walled glass vessel with constant overhead stirring (Metrohm 802). The working solutions were prepared by mixing appropriate amounts of 0.1 M $CaCl_2$ and 0.1 M $NaHCO_3$ solutions with 0.1 M NaCl solution to obtain the desired supersaturation with respect to calcite. The ionic strength was maintained by 0.1 M NaCl solution in all experiments. At pH 8.5, small portion of powdered chalk sample (0.05 – 0.15 g) was added to the working solution to initiate precipitation. When calcite begins to precipitate, pH of the solution drops. This is compensated by titrating $CaCl_2$ and Na_2CO_3 / $NaHCO_3$ solutions using a peristaltic pump and conditions for calcite precipitation is keeping steady state. For all types of precipitation experiments, we used five supersaturation values, S: 2.40, 3.02, 3.87, and 4.50, corresponding to Ca concentrations (total Ca = total carbonate) in the working solution of 2.0, 2,7, 3.3, and 4.0 mM. Supersaturation, *S*, was defined as

$$S = \left(\frac{IAP}{K_{sp}} \right)^{1/2} = \left(\frac{a_{Ca^{2+}} a_{CO_3^{2-}}}{K_{sp}} \right)^{1/2},$$

where IAP represents the ion activity product in the actual solution, a_{ion}, ion activity and K_{sp}, the thermodynamic solubility product of calcite.

A typical plot of the rate of titrant addition for the precipitation experiments is shown in Fig. 1. Our attention was focused on the initial part of the curve (0.5 - 3 min after the onset of precipitation, depending on supersaturation), which correlates with calcite precipitation on the original chalk particle surfaces. Thereafter, calcite could grow on newly precipitated calcite. This effect can be seen in Fig. 1, where the rate of titrant addition, hence the calcite precipitation rate, dramatically increased with time.

The overall precipitation rate, *R*, is determined as follows:

$R = \frac{[Ca]_{titr}}{mA} \frac{dV}{dt} = \frac{[Ca]_{titr}}{mA} R'$, where R' represents the solution addition rate, $[Ca]_{titr}$, Ca concentration in the titrant $CaCl_2$ solution, *m*, the initial seed mass, *A*, the specific surface area and *V*, the volume of the titrant added.

Calcite precipitation rate for the various chalk samples as a function of log(S-1) are summarized in Fig. 2. Here, for comparison, calcite precipitation rate for experiments using the Sigma calcite seeds are shown for comparison (Lakshtanov et al., 2011; Karaseva et al., 2018).

For calcite precipitation on the calcite seeds, a plot of the precipitation rate vs. relative supersaturation (Fig. 2) satisfactorily fits the experimental data with the apparent reaction order (slope of the line) n = 1.8, $f(S) = (S-1)^{1.8}$, which indicates nearly parabolic dependence of precipitation rate on relative supersaturation over the whole range of supersaturation examined in the present study. This means that the rate determining step for calcite growth is the surface diffusion of the growth units (Burton et al., 1951).

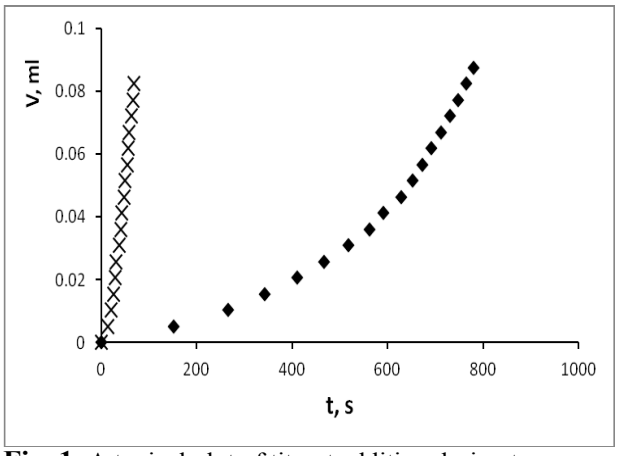

Fig. 1. A typical plot of titrant addition during two precipitation experiments (chalk 10-4, rhombi *S*=2.4; crosses *S*=4.5).

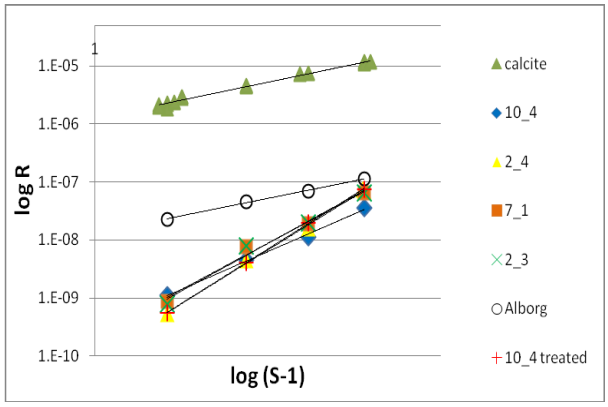

Fig. 2. Rate of calcite precipitation on the various chalk samples as a function of relative supersaturation (data for calcite (Lakshtanov et al., 2011; Karaseva et al., 2018). The lines were calculated by linear regression of the data.

For all chalk samples (Fig.2), at low supersaturation, calcite precipitation rate is 3 orders of magnitude lower than that for pure calcite. For Ålborg chalk, which has been in the freeze-thaw zone, exposed to groundwater flow for 10,000 years, precipitation rate is 2 orders of magnitude lower. Also for all chalk samples (except Ålborg chalk), the apparent reaction order, *n*, ranged between 3.7 and 5.4, which is much higher than 2. This means that calcite precipitation on the original chalk particle surfaces is by (at least mostly) surface nucleation mediated growth:

$f(S) = (S-1)^{2/3} S^{1/3} \exp(-B_{2D} / 3\ln S)$ for two-dimensional nucleation-mediated growth. In this equation, B_{2D} is the free energy barrier for creating the new step edge:

$B_{2D} = \frac{\beta \kappa^2 a}{2k^2 T^2}$, where β represents a shape factor (π for circles), κ (J m^{-1}) represents an effective edge free energy and a, the molecular area.

For Ålborg chalk, n = 1.7, so calcite precipitation on these particles is much slower but it is described nearly by the parabolic law, as for calcite. Following extraction of the nonpolar organic material from Chalk sample 10-4, the reaction order, n, increased from 3.7 to 5.4, i.e. indicating growth by surface nucleation.

We determined the ζ potential for the chalk samples to gain better understanding about the interactions that occur at the chalk surface. The values of ζ-potential were calculated from the streaming potential measurements using the Helmholtz - Smoluchowski:

$$\zeta = \frac{dU}{dp} \times \frac{\eta}{\varepsilon \times \varepsilon_0} \times \kappa_B ,$$

where ζ – zeta potential, dU/dp – slope of streaming potential versus pressure, η – electrolyte viscosity, ε_0 – vacuum permittivity, ε – dielectric constant of electrolyte and κ_B – specific electrical conductivity of the electrolyte.

For streaming potential measurements, the cylindrical cell was used. Electrolyte solution was pumped through the sample cell with a pressure gradually increasing up to 300 mbar. The dependence of ζ-potential on pH was measured in the pH range 6.0 – 10.0 and an average value between 4 measurements was calculated. In all measurements, the chalk-saturated 1 mM NaCl solution was used. The titration was performed using 0.1 M solutions of HCl and NaOH by the automatic titration procedure. Streaming potential measurements were made in the solution saturated with the corresponding chalk, with addition of 0.001 M NaCl, at equilibrium with atmospheric CO_2. In these experiments, we also included the chalk samples (2-3) that had been treated with H_2O_2 (2-3 t), with the intention of removing polysaccharide polymers from the chalk surface. ζ potential for pure calcite seed at pH < 8.5 is slightly positive and becomes negative at higher pH (Fig. 3).

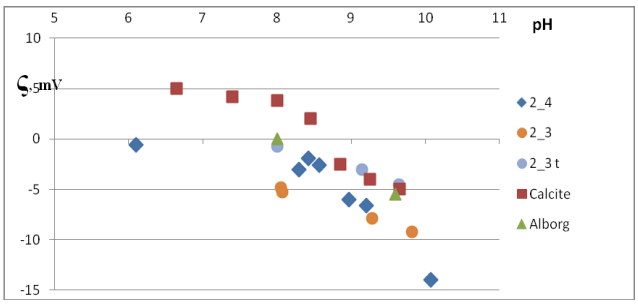

Fig. 3. pH dependence of ζ potential for calcite and the chalk samples. Chalk sample 2-3 t had been treated with H_2O_2 (Belova et al., 2018).

Such behaviour is consistent with the surface speciation model of the calcite-water interface (Pokrovsky et al., 2000), which predicts a point of zero charge at pH = 8.2 on the basis of the electrokinetic measurements (Mishra, 1978). Chalk samples have negative ζ potential, much more negative than for pure calcite. There is considerable evidence in the literature that the ζ potential of calcite, including natural samples (e.g. chalk), as well as synthetic calcite, clearly reflects the effect of

organic compound adsorption. Organic molecules reduce the positive surface charge of calcite and reverse it to negative (Cicerone et al., 1992, Vdović, 2001, Karaseva, 2018). Comparison of the ζ potential for chalk samples with calcite indicates insignificant contribution of electrostatics to the interaction energy. Because the pK_a of carboxylate polysaccharides is usually < 5 (Shinde and Nagarsenker, 2009), the molecules are deprotonated, thus anionic in the pH range > pK_a. Since at pH > 8.5, both the calcite surface and the deprotonated polysaccharides are negatively charged, and they adsorb independently of their charge, the electrokinetic measurements testify to the specific, coordinative interaction between the functional groups of organic molecules and the calcite surface. Such specific adsorption is the main reason for strong inhibition of calcite precipitation by the polysaccharides and certain other organic compounds.

So, we observed the relationship between precipitation rate and supersaturation to determine the active mechanism of calcite precipitation on particle surfaces from a number of different chalk samples. Our results show that the rate of calcite precipitation on the surface of chalk samples does not obey the parabolic law that is characteristic for calcite growth. Instead, the dependence of calcite precipitation rate on supersaturation is exponential, which indicates surface nucleation mediated growth. The rates of calcite precipitation on the chalk particle surfaces at the lowest supersaturation investigated in the present work are three orders of magnitude lower than for pure calcite. This means that during chalk recrystallization, which is one of the dominant processes in burial diagenesis, when supersaturation is extremely low, recrystallization can be significantly suppressed. This, along with other possible causes of inhibition, can be responsible for the extremely slow rates for chalk recrystallization. The date obtained by determination of the ζ potential for the chalk samples show that the specific adsorption is the main reason for strong inhibition of calcite precipitation by the polysaccharides and certain other organic compounds.

References:

Fabricius, I.L., Borre, M.K., 2007. Stylolites, porosity, depositional texture, and silicates in chalk facies sediments. Ontong Java Plateau – Gorm and Tyra fields, North Sea. Sedimentology 54, 183–205.

Lakshtanov, L.Z., Bovet, N., Stipp, S.L.S., 2011. Inhibition of calcite growth by alginate. Geochim. Cosmochim. Acta 75, 3945−3955.

Montanari, G., Lakshtanov, L.Z., Tobler, D.J., Dideriksen, K., Dalby, K.N., Bovet, N., Stipp, S.L.S., 2016. Effect of Aspartic Acid and Glycine on Calcite Growth. Crystal Growth Des. 16, 4813-4821.

Karaseva, O.N.; Lakshtanov, L.Z.; Okhrimenko, D.V.; Belova, D.A.; Generosi, J.; Stipp, S.L.S. Biopolymer control on calcite precipitation. // Cryst. Growth Des. 2018. Vol. 18, № 5, P. 2972-2985.

Burton, W.K., Cabrera, N., Frank, F.C., 1951. The growth of crystals and the equilibrium structure of their surfaces. Phil. Trans. R. Soc. A. 243, 299–358.

Pokrovsky, O.S., Mielczarski, J.A., Barres, O., Schott, J., 2000. Surface speciation models of calcite and dolomite/aqueous solution interfaces and their spectroscopic evaluation. Langmuir 16, 2677-2688.

Mishra, S.K., 1978. The electrokinetics of apatite and calcite in inorganic electrolyte environment. Int. J. Miner. Process. 5, 69-83.

Cicerone, D.S., Regazzoni, A.E., Blesa, M.A., 1992. Electrokinetic properties of the calcite/water interface in the presence of magnesium and organic matter. J. Colloid Int. Sci. 154, 423-433.

Vdović, N., 2001. Electrokinetic behaviour of calcite—the relationship with other calcite properties. Chem. Geol. 177, 241-248.

Shinde, U.A.; Nagarsenker, M.S. Characterization of Gelatin-Sodium Alginate Complex Coacervation System. Indian J. Pharm Sci. 2009, 71, 313–317.

Redkin A.F., Kotova N.P. Experimental study of pyrochlore solubility in NaF solutions at 800°C, 170–230 MPa.

Institute of Experimental Mineralogy RAS, Chernogolovka, Moscow district (redkin@iem.ac.ru, kotova@iem.ac.ru)

Abstract. Preliminary data on pyrochlore solubility in NaF solutions at 800°C, 170-230 MPa are obtained. It is shown that pyrochlore solubility in NaF solutions is 10-30 times higher than that of microlite. It is found that at the immiscibility boundary (HS-I → L_1+L_2), an abrupt increase in the solubility of pyrochlore is observed.

***Keywords**: experiment, pyrochlore, solubility, fluoride solutions*

Pyrochlore is the main niobium - containing ore mineral, therefore the study of its behavior in hydrothermal and magmatic systems is of interest for the genesis of the corresponding rare metal deposits. Niobium - and tantalum-containing ore minerals have low solubility in hydrothermal solutions, so it is believed that their formation is associated with the evolution of fluorine-containing magmatic melts. However, in a number of works (Zaraisky et al., 2010; Korzhinskaya, Kotova, 2012; Redkin, Kotova, 2016) there was shown that fluoride solutions are able to accumulate significant concentrations of niobium and to participate in the recrystallization of rare metal ores The predominant form niobium transfer are fluoride complexes. Of particular interest are solutions of sodium fluoride, since sodium is the dominant cation of most hydrothermal solutions of magmatogenic genesis.

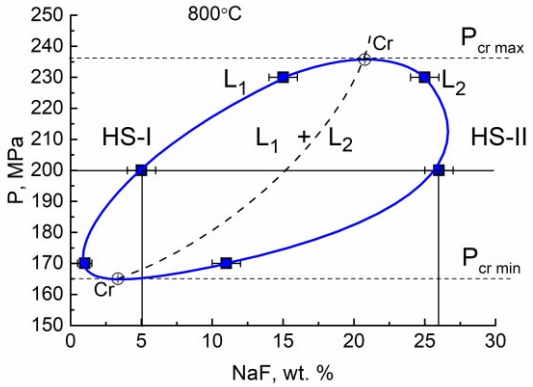

Fig. 1. Fluid immiscibility region ($L_1 + L_2$) in the NaF-H_2O system at 800° C

The solubility of pyrochlore (Pcl - $(NaCa)Nb_2O_6F$ was studied in solutions containing 0.1-16 m NaF, covering both the homogeneous solution region (HS-I and HS-II) and the fluid immiscibility region (L_1+L_2) in the NaF-H_2O (Figure 1). In the NaF- H_2O system at 800°C there is a limited region of immiscibility of solutions (Redkin et al., 2016), in which a feature of NaF hydrolysis, affecting the solubility of the ore mineral, is manifested. The immiscibility region (L_1+L_2) is contoured by the results of a study of microlite, $(NaCa)Ta_2O_6F$ solubility, in NaF solutions. At 800°C and 170, 200, and 230 MPa, the NaF content in the L_1 and L_2 fluid phases is 1 and 11 wt. %, 5 and 26%, 12 and 25% respectively. Because pyrochlore, as will be shown below, has a low solubility, the boundaries of the fluid immiscibility cannot change significantly and all inconsistencies can be related to the experimental procedure, primarily the accuracy of the temperature and pressure setting in the reaction zone.

The experiments were performed in a gas vessel, while 4-5 capsules were placed together into the container, and also on a hydrothermal line in reactors with a diameter of 6-8 mm. The quenched aqueous solutions were then analyzed using ICP/MS (Inductively Coupled Plasma Mass Spectrometry) and ICP/AES (Atomic Emission Spectroscopy). The composition of the solid product was characterized using X-ray diffraction, and electron microprobe analysis (Cam Scan MV 2300 (VEGA TS5130MM).

Pyrochlore (Pcl) and fluorite (Flu) were present in the solid run products. Experimental data on the solubility of pyrochlore as a function of the total concentrations of NaF are shown in Figure 2.

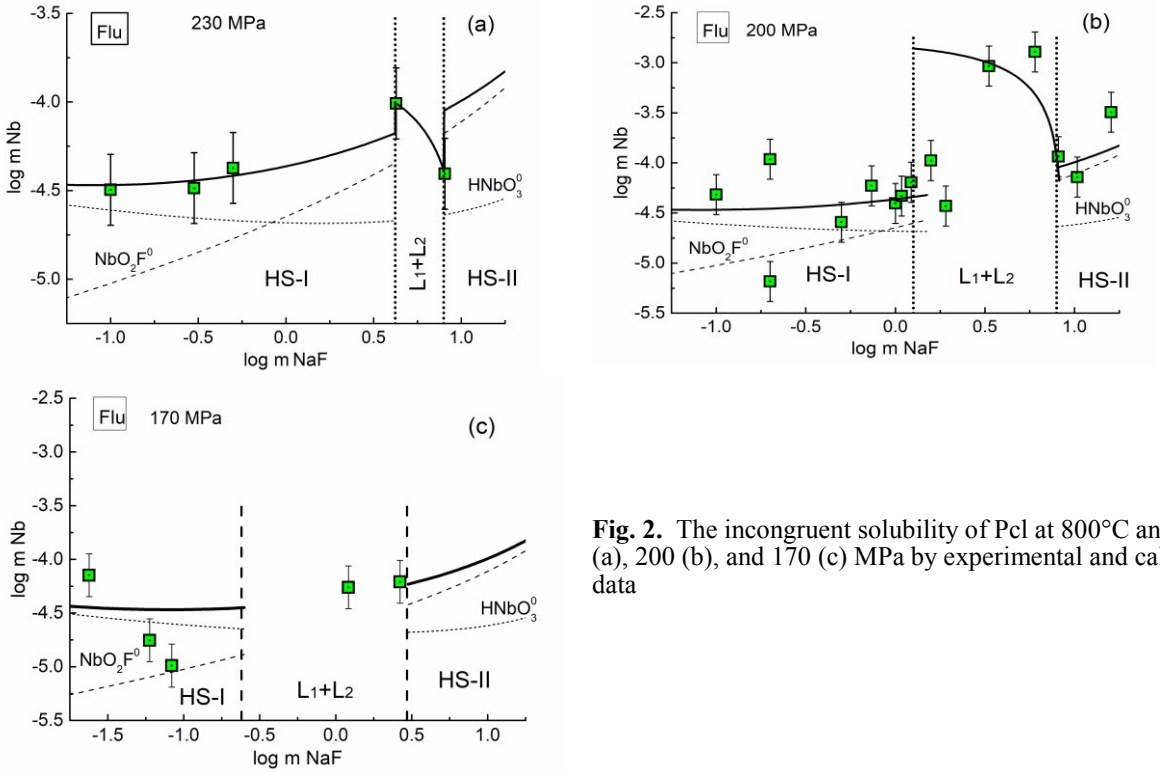

Fig. 2. The incongruent solubility of Pcl at 800°C and 230 (a), 200 (b), and 170 (c) MPa by experimental and calculated data

The obtained experimental data were used to determine the main forms of Nb^{5+} transport in fluoride solutions. The calculations were performed according to the OptimA program (Shvarov, 2015). It was established that the main forms of niobium in the fluoride solutions studied could be species of $HNbO_3^0$ and NbO_2F^0. Other species, $NbOOHF_2^0$, $Na_6H_2Nb_6O_{19}^0$, and $NaNbO_3$, similar to those founded for tantalum, are present in small amounts. As a result of the thermodynamic calculations, the reaction constants are determined:

$Pcl+2HF^0 + H_2O = Flu+2HNbO_3^0+NaF^0$ (1),

$\lg K_p(1) = -7.27$

$Pcl+4HF^0 = Flu+2NbO_2F^0+NaF^0+2H_2O$ (2),

$\lg K_p(2) = -2.60$

In Figure 2 the concentrations of $HNbO_3^0$ and NbO_2F^0 species are shown by dashed lines, and the total concentration of niobium in homogeneous solutions is shown by a solid line. Experimental data indicate the feature of the change in pyrochlore solubility in the fluid immiscibility region - the apparent solubility of pyrochlore decreases with increasing total NaF concentration. According to the studies, it was established that in the homogeneous region of NaF solutions the concentration of niobium in equilibrium with Pcl + Flu is in the range from $3 \cdot 10^{-5}$ to $3 \cdot 10^{-4}$ mol/kg H_2O, which is 10-30 times higher than the concentration tantalum in equilibrium with microlite and fluorite (Redkin et al., 2016)

This work was supported by the grants of RFBR 18-05-01001-a

References:

Zaraisky, G. P., Korzhinskaya, V., and Kotova, N. 2010. Experimental studies of Ta_2O_5 and columbite–tantalite solubility in fluoride solutions from 300 to 550°C and 50 to 100 MPa. *Miner. Petrol.* 99: 287–300. DOI 10.1007/s00710-010-0112-z.

Korzhinskaya, V.S., Kotova N.P, 2012. Experimental modeling of the possibility of niobium hydrothermal transport via fluoride solutions. BULLETIN OF INSTITUTE OF RAS, VOLUME 4, NZ9001, doi: 10.2205/2012NZ_ASEMPG, 2012.

Redkin A.F., Kotova N.P. 2016. Effect of the concentration of NaF on the solubility of pyrochlore at 800°C, 200 MPa. Materials of the XVII International Conf.: Physical-Chemical and Petrophysical Studies in the Sciences of the Earth. Moscow-Borok, September 26-30. 2016. Moscow, p. 290-292.

Redkin A.F., Kotova N.P. , and Shapovalov Yu. B. 2016. Liquid immiscibility in the system NaF–H_2O and microlite solubility at 800°C. *Doklady Earth Sciences* 469(1): 722-727. DOI: 10.1134/S1028334X16070151.

Shvarov, Yuri. (2015). A suite of programs, OptimA, OptimB, OptimC, and OptimS compatible with the Unitherm database, for deriving the thermodynamic properties of aqueous species from solubility, potentiometry and spectroscopy measurements. *Applied Geochemistry*, *55*, 17-27. http:// dx.doi.org/ 10.1016/ j.apgeochem. 2014.11.021.

Tauson V.L.[1], Smagunov N.V.[1], Lipko S.V.[1], Loginov B.A.[2], Popovich A.A.[2], Baranov G.V.[2], Knyazev M.I.[2] Cocrystallization coefficients of elements of fe group and al in magnetite and hematite and the effect of superficial segregation UDC 550.42 + 553.21/24

[1]A.P.Vinogradov Institute of Geochemistry, SB RAS, Irkutsk (vltauson@igc.irk.ru),
[2]National Research University "Moscow Institute of Electron Technology", Zelenograd

Abstract. The experiments were carried out by a growth scheme using the internal sampling of fluid at 450°C and 100 MPa. The crystal phases obtained were studied by the methods of electron probe microanalysis (EPMA), mass spectrometry with inductively coupled plasma and laser ablation (LA-ICP-MS), atomic absorption spectrometry (AAS), scanning probe microscopy (SPM in AFM and STM modes), X-ray photoelectron spectroscopy (XPS). The solutions from samplers were analyzed by AAS. The highest cocrystallization coefficients $D_{Me/Fe}$ in magnetite characterize Ni, V, Al and Cr (order of units), lower value was observed for Co (0.2), and still lower for Ti, Zn and Mn ($n \cdot 10^{-2} – 10^{-3}$). In hematite, $D_{Me/Fe}$ values are maximal for Al, V and Ti. Copper is approved as a most incompatible in both minerals ($2 – 3 \cdot 10^{-5}$). Nevertheless, Cu reveals high content belonging to the crystal surface. The superficial segregation provides a significant contribution to the average trace element concentration even at low thickness of superficial phase enriched in the element. The results of the present study show that the data on trace element partitioning obtained with bulk analytical methods should be carefully revisited especially when small crystals with uncontrolled sizes were used in experiments.

Keywords: *Fe group elements, Al, distribution, hydrothermal solution, magnetite, hematite, crystal surface, trace element segregation*

Introduction. Cocrysalllization coefficients of elements A and B ($D_{A/B}$) are the most important characteristics, which control the partitioning and distribution of elements in geochemical processes. In the absence of information on their numerical values, it is difficult to identify the fundamental causes of differentiation of chemically similar elements and common geochemical paths of chemically different elements. This information would enable quantitative identification of minerals, which contribute to partition of different elements in various processes. The ratio of elements in the ore-forming fluid is objectively reflected in the composition of the mineral solid solution crystallized from this fluid; therefore, the information on $D_{A/B}$ values will provide evaluations of elements concentration proportions in mineral-forming media. Magnetite (Fe_3O_4) as a "transient" mineral of variable composition, capable to isomorphous incorporation of many elements, is a promising object of such study. Magnetite is found in a variety of geological objects, from ultramafites to granitic rocks and metamorphic rocks of different facies and compositions (Ilton, Eugster, 1990). Study and use of typochemistry of magnetite and other spinelides at the level of the quantitative models is hardly possible without the data on the constants of elements distribution between their crystals and solutions. This is important not only in theory but also in practical aspect, since minerals of this group, due to the peculiarities of their composition, are used as geochemical prospecting indicators of certain ore types, as exemplified by gahnite (Zn^{2+}, Fe^{2+}, Mg^{2+}) [Al^{3+}, Fe^{3+}]$_2$ O_4 (O'Brien et al., 2015). Hematite (α-Fe_2O_3) is a characteristic component of secondary geochemical media; it often accompanies magnetite and participates in the redistribution of elements under its oxidation.

Experimental and analytical methods. There was applied a technique of hydrothermal thermogradient synthesis of crystals in passivated titanium inserts at 450°C and the pressure of 100

MPa (1 kb) with 15-degree temperature drop on the external wall of the autoclave, in solutions based on ammonium chloride (Tauson et al., 2017 a, b). Internal fluid sampling in perforated titanium traps was applied. In the experiments Fe form ratios (II, III, and 0) and impurity components content in the batch varied, as well as the concentration of the mineralizing solution. This was done to identify the most sustainable element indicators, for which the $D_{Me/Fe}$ is less dependent on the complexity of the system, the fO_2 and other parameters. The duration of the experiments was 4 days in isothermal mode and 20 days in gradient mode. The crystalline phases obtained (magnetite, Ni-spinel, hematite) were analyzed by different methods. Electron probe microanalysis (EPMA) was performed on the Superprobe JXA-8200 (JEOL Ltd, Japan) unit in the Institute of Geochemistry SB RAS. The method of mass spectrometry with inductively coupled plasma and laser ablation (LA-ICP-MS) was implemented on Agilent 7500ce (Limnological Insitute SB RAS) and Perkin Elmer NexION 300D units (Institute of Geochemistry SB RAS) with the laser ablation platform NWR-213 (United States). Analysis by the method of atomic absorption spectrometry (AAS) was carried out on Perkin-Elmer M403 and M503 (United States) units, X-ray diffraction analysis (RDA) – on D8 ADVANCE diffractometer manufactured by BRUKER (Germany) in the Institute of Geochemistry SB RAS. The study of the crystals surface by the method of scanning probe microscopy (SPM) in atomic force microscopy (AFM) and scanning tunneling microscopy (STM) modes was performed on Russian scanning multimicroscopes CMM-2000 of various modifications in the Institute of Geochemistry SB RAS and NRU "Moscow Institute of Electronic Technology", as well as by the method of X-ray photoelectron spectroscopy (XPS) on SPECS spectrometer with energy analyzer PHOIBOS 150 MCD 9 (Germany) in the Krasnoyarsk regional Centre for collective use of SB RAS.

Results. In the experiments there were obtained sufficiently large (up to 3 mm) crystals of magnetite (Mt) and smaller (up to 1 mm) crystals of nickel spinel (Sp) and hematite (Hm). In some experiments, Mt and Hm were obtained together in various proportions. Ni–Sp differs from magnetite by higher content of Ni and lower unit cell parameter (a_0 = 0.835-0.836 nm) compared to magnetite containing the same basic impurities (Ni and Co), but in lower concentrations (a_0 = 0.838 – 0.840 nm). EPMA study identified a sample with a very uniform distribution of Ni and Co, which was used as an external standard in the analysis by LA-ICP-MS method. These two elements determined by EPMA in each of the analyzed grains of each sample were used as internal standards for the analysis in the same grains of other elements present in concentrations below the minimum detection limit (MDL EPMA ~ 0.1 wt.%), but available for determination by the method of LA-ICP-MS (MDL ~ 1 ppm for most impurity elements). Fig. 1 presents the mean values of the cocrystallization coefficients of the studied elements in Mt, Sp and Hm, their variations are given with the confidence level of 90%.

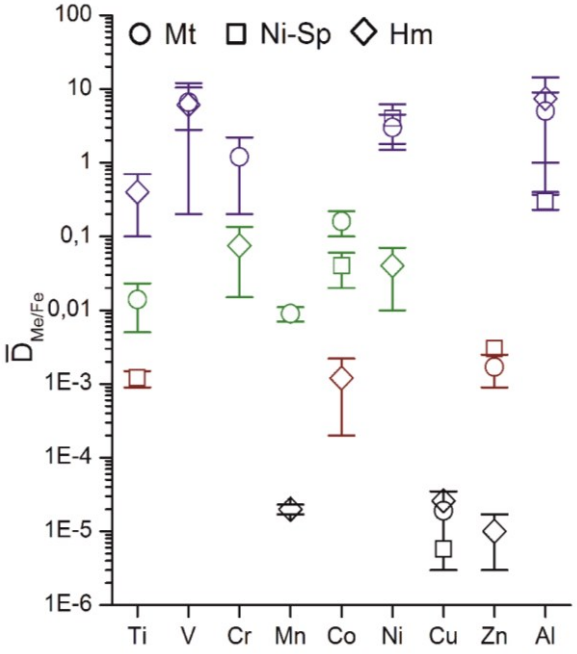

Fig. 1. Cocrystallization coefficients of iron group elements and aluminum in magnetite, Ni-spinel and hematite. The same color marks the points for elements and minerals with similar D.

The reliable data set was obtained for magnetite; the data for Ni-spinel and hematite are fragmentary and are preliminary in nature. As the figure shows, Co, Ni and Mn are characterized by smaller variances of $D_{Me/Fe}$ and can therefore be considered as the most resistant to change in environmental parameters and the system composition, which means that these elements may be recommended as indicators of the composition of mineral forming fluids.

Highly coherent elements in magnetite are Ni, Al, V, Cr and Co. Titanium demonstrates unstable behavior and, along with zinc and manganese, falls under the category of weakly incoherent elements in magnetite. Highly coherent elements in hematite are Al, Ti, V, and, to a lesser extent Cr and Ni, slightly incompatible is Co, the most incoherent elements in hematite are Zn, Mn and Cu.

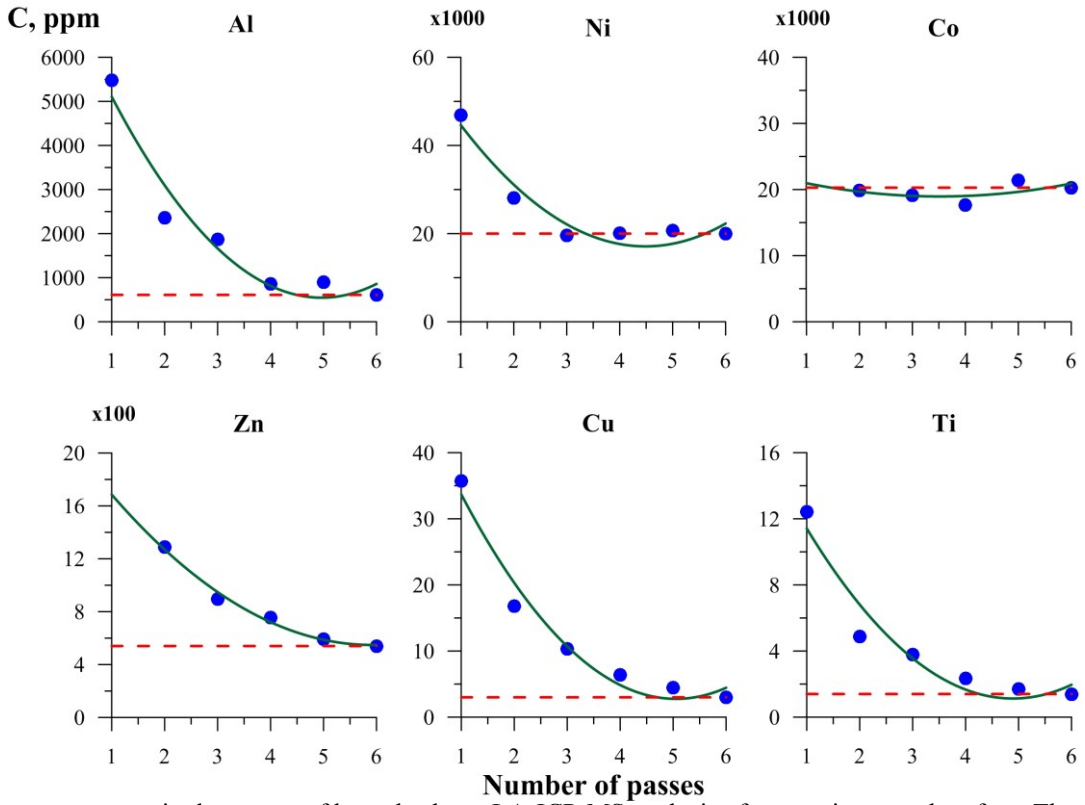

Fig. 2. Elements content in the course of layer-by-layer LA-ICP-MS analysis of magnetite crystal surface. The first 2-3 laser passages detect higher contents of the elements in respect of the volume concentration (dotted line).

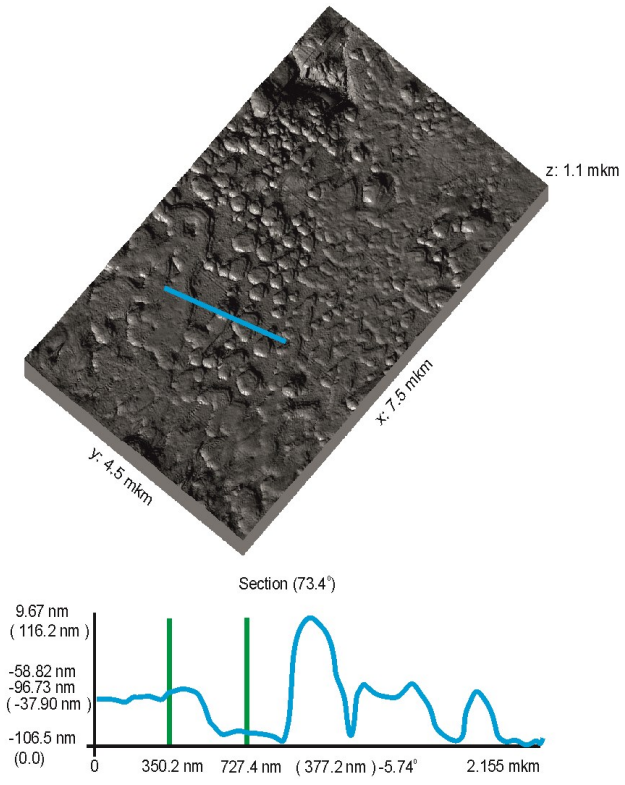

Fig. 3. Atomic force mode image of magnetite crystal surface with the cross-section of surface sector profile.

In the process of research it was found that some elements demonstrate lack of correlation between the AAS data and the data obtained by local methods. This is dramatically evident in the case of copper: based on AAS results, its contents in the crystals range from 30 up to 3500 ppm, whereas according to EPMA they are much below MDL, and LA-ICP-MS detects only 2.7 – 17 ppm Cu in all the three minerals. This proved to be caused by the same phenomenon we repeatedly faced when studying distribution of noble metals – Au, Pt, Pd (Tauson, et al. 2017a), namely, absorption of trace element by surface non-autonomous phase (SNAP). Figure 2 shows the results of layer-by-layer LA-ICP-MS analysis in 6 laser passages. As we can see, the first 2-3 passages show markedly higher contents than those in volume (dotted line). This is not so relevant for macroelements (Ni, Co), but is clearly identified for microelements (< ~ 0.1%).

It proved very difficult to standardize the depth of the passage due to the high surface roughness in laser track. According to preliminary estimates, SNAP thickness does not exceed 300 nm. Figure 3 presents AFM image of one of the magnetite crystal surface sectors, indicating the presence of objects up to ~ 100 nm high on the surface. This does not contradict XPS data with Ar+ ion etching of surface, according to which SNAP has oxyhydroxide composition and apparently implements the potential of goethite-like phases to structural incorporation of elements of iron group and aluminum (Wells et al., 2006). XPS spectra of Fe 2 p and O 1s show that SNAP compositions on the surface of Mt and Hm do not differ significantly; they both contain OH^- group and Fe^{3+} and Fe^{2+} in the proportion ~ 1:1. These data were obtained on the basis of multiplet

decomposition of the spectra, taking into account not only charge state of Fe, but also its spin state.

STM images show that there are relief peculiarities at a lower dimension level (Fig. 4), which speaks in favor of fractal nature of the surface. It is important for the absorption of microelements by SNAP, as it points to the increase of the real surface as compared to the topological one.

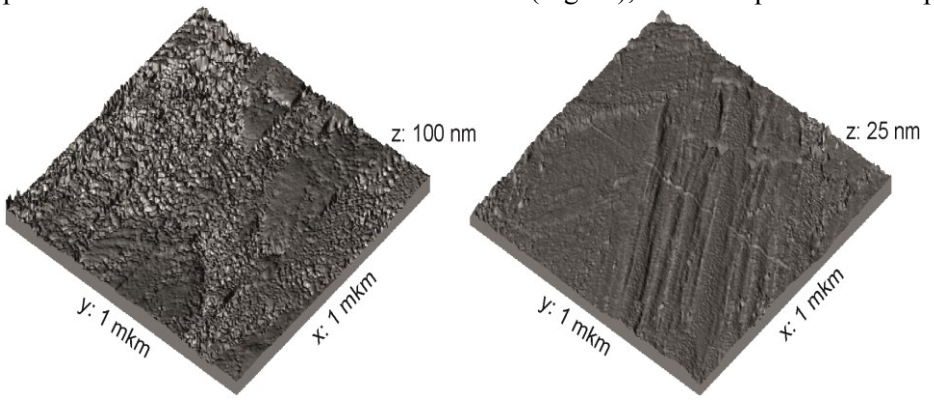

Fig. 4. High resolution images of magnetite crystals surface in the scanning tunneling microscope.

Discussion of the results. As Fig. 1 shows, Co, Ni and Mn are characterized by smaller D variances as compared to other elements and can be recommended as indicators of the composition of mineral-forming fluids. The stability of Co and Ni behavior is proven by the fact that the data on these elements are consistent for magnetite and nickel spinel, which are dramatically different in composition. Other elements are more susceptible to medium peculiarities and system composition. These data also suggest that Mt oxidation and its transition to Hm in hydrothermal medium will cause the release of Co, Ni, Zn, Mn and Cr, practically will not affect the behavior of Cu, Al, and V, and will facilitate the Ti absorption by the solid phase. Quite a lot of data on the composition of magnetite and hematite of various geneses have been accumulated by now; nevertheless, this information is of little relevance due to the absence of ways of transition from them to the composition of the ore-forming fluid. Using the $D_{Me/Fe}$ data obtained, we calculated the proportion of elements in the fluid, which forms magnetite composition at the iron-ore with sulfides (principally pyrite and pyrrhotite) deposit Cihai (Tian Shan, Northwest China) (Huang et al., 2013). The results for 6 samples are presented in the Table. Its data lead to the conclusion that Mn and Zn in the solutions are present in comparable concentrations (Zn/Mn ~ 1.3), and are essential components of the fluid, accounting for approximately 1/3 of Fe content. Fluid macrocomponents may include Cu, which is identified in one sample only. Secondary (minor) elements of the fluid are Ti and Al amounted to the hundredths and thousandths of Fe content. Fluid microelements may be split into two groups: Co and Ni are ten thousandth and hundred thousandth of Fe content, V and Cr – millionth parts.

Table. Atomic proportions $(Me/Fe)^{aq}$ calculated on the basis of obtained $D_{Me/Fe}$ and the data of LA-ISP-MS for magnetites of magmatogenic-hydrothermal deposit Cihai (Tien Shan, SW China) (Huang et al., 2013)

Dominating components (contents are comparable with Fe by the order-of-magnitude)		
Zn	Mn	(Cu?)*
0.41 ± 0.06	0.32 ± 0.06	0.13
Minor components		
Ti	Al	
$(5.2 \pm 2) \cdot 10^{-2}$	$(5.2 \pm 1.2) \cdot 10^{-3}$	
Fluid microcomponents		
Co	Ni	V	Cr
$(5.8 \pm 0.6) \cdot 10^{-4}$	$(2.0 \pm 0.3) \cdot 10^{-5}$	$(8.5 \pm 3) \cdot 10^{-6}$	$(6.0 \pm 0.8) \cdot 10^{-6}$

* Detected in a single sample.

Conclusion. The experiments were conducted according to the growth scheme using internal sampling at 450°C and 100 MPa. The highest cocrystallization coefficients of $D_{Me/Fe}$ in magnetite were established for Ni, V, Al and Cr (first whole shares); the value for Co was significantly lower (0.2); with even lower figures for Ti, Zn and Mn ($n \cdot 10^{-2} – 10^{-3}$). In hematite these values are the highest for Al, V and Ti (7, 6, and 0.4 respectively), they are significantly lower for Ni and Co ($n \cdot 10^{-2} – 10^{-3}$), compared with magnetite. Copper proved to be the most incompatible element in both minerals ($2–3 \cdot 10^{-5}$). However, it demonstrates high concentrations on crystal surface. Surface segregation provides a significant contribution to the average concentration of microelement even with a low thickness of the surface phase enriched with it. The data obtained show that one needs to be very careful with the

results acquired by bulk analysis methods, with the crystal size being small enough and beyond control. Co, Ni and Mn were found to be characterized by lower variances D as compared to other elements and can be recommended as indicators of the composition of mineral forming fluids. Restoration of fluid composition by the composition of magnetite of one of the iron ore deposits of magmatogenic-hydrothermal genesis revealed that its primary components might be presented by Zn, Mn and, possibly, Cu; the secondary ones – Ti and Al, microelements – Co, Ni, V and Cr.

The study was performed within the framework of the state order on the Project IX.125.3, No. 0350-2016-0025 and was supported by RFBR, grants 18-05-00077, 16-05-00104.

The authors are deeply grateful to D.N. Babkin and T.M. Pastushkova for participation in the organization of the experiments and analysis of the material. In the course of the study, we used the equipment of Common Use Centre (CUC) "Isotope-geochemical studies" of the Institute of Geochemistry, SB RAS, and CUC «Ultramikroanaliz» of the Limnological Institute SB RAS.

References:

Tauson V.L., Lipko S.V., Arsentev K.Yu., Mikhlin Yu.L., Babkin D.N., Smagunov N.V., Pastushkova T.M., Voronova I.Yu., Belozerova O.Yu. Dualistic distribution coefficients of trace elements in the system mineral–hydrothermal solution. IV. Platinum and silver in pyrite // Geochemistry International. 2017a. Vol. 55. № 9. P. 753-774.

Tauson V.L., Smagunov N.V., Lipko S.V. Cocrystallization coefficients of Cr, V, and Fe in hydrothermal ore systems (from experimental data) // Russian Geology and Geophysics. 2017b. Vol. 58. № 8. P. 949-955.

Ilton E.S., Eugster H.P. Partitioning of base metals between silicates, oxides, and a chloride- rich hydrothermal fluid. Part 1. Evaluation of data derived from experimental and natural assemblages // In: Fluid-Mineral Interactions: A Tribute to H.P.Eugster. Eds. R.J.Spencer and I-Ming Chou. Geochem. Soc. Spec. Pub. 1990. № 2. P. 157-169.

Huang X.-W., Zhou M.-F., Liang Q., Gao J.-F., Wang Y.-W. Re-Os isotopic ages of pyrite and chemical composition of magnetite from the Cinai magmatic-hydrothermal Fe deposit, NW China // Miner. Deposita. 2013. Vol. 48. P. 925-946.

O'Brien J.J., Spry P.G., Teale G.S., Jackson S.E., Koenig A.E. Gahnite composition as a means to fingerprint metamorphosed massive sulfide and non-sulfide zinc deposits // J. Geochem. Explor. 2015. Vol. 159. P. 48-61.

Wells M.A., Fitzpatrick R.W., Gilkes R.J. Thermal and mineral properties of Al-, Cr-, Mn-, Ni-, and Ti-substituted goethite // Clays Clay Miner. 2006. Vol. 54. № 2. P. 176-194.